Passive offsetting of CO_2 emissions at the Mount Keith Nickel Mine, Western Australia: A basis for geoengineering carbon neutral mines

Siobhan A. Wilson[a,b]*, Anna L. Harrison[b], Gregory M. Dipple[b], Ian M. Power[b], Shaun L.L. Barker[c], K. Ulrich Mayer[b], Stewart J. Fallon[d], Mati Raudsepp[b] and Gordon Southam[e]

[a]School of Geosciences, Monash University, Clayton, Victoria 3800, Australia.

[b]Mineral Deposit Research Unit, Department of Earth, Ocean and Atmospheric Sciences, The University of British Columbia, 2207 Main Mall, Vancouver, British Columbia V6T 1Z4, Canada.

[c]Department of Earth and Ocean Sciences, The University of Waikato, Hamilton 3240, New Zealand.

[d]Research School of Earth Sciences, The Australian National University, Canberra, Australian Capital Territory 0200, Australia.

[e]School of Earth Sciences, The University of Queensland, St Lucia, Queensland 4072, Australia.

*Corresponding author. email: sasha.wilson@monash.edu; tel: +61 3 9905 1119; fax: +61 3 9905 4903.

Abstract

The hydrated Mg-carbonate mineral, hydromagnesite [$Mg_5(CO_3)_4(OH)_2{\cdot}4H_2O$], precipitates within mine tailings at the Mount Keith Nickel Mine, Western Australia as a direct result of mining operations. We have used quantitative mineralogical data and $\delta^{13}C$, $\delta^{18}O$ and $F^{14}C$ isotopic data to quantify the amount of CO_2 fixation and identify carbon sources. Our radiocarbon results indicate that at least 80% of carbon in hydromagnesite is sourced from the modern atmosphere. Stable isotopic results indicate that dissolution of atmospheric CO_2 into mine tailings water is kinetically limited, which suggests that the passive rate of carbon mineralization could be accelerated. Reactive transport modeling is used to describe the observed variation in tailings mineralogy and to estimate rates of CO_2 fixation. Based on our assessment, approximately 39 800 t/yr of atmospheric CO_2 are being trapped and stored in tailings at Mount Keith. This represents an offsetting of approximately 11% of the mine's annual greenhouse gas emissions. Thus, passive sequestration via enhanced weathering of mineral waste can capture and store a significant amount of CO_2. Implementation of geoengineering strategies that accelerate the uptake of CO_2 into tailings water could further reduce or completely offset the net greenhouse gas emissions at Mount Keith and many other mines.

Keywords: Enhanced weathering; mineral carbonation; Mount Keith Nickel Mine; reactive transport modeling; stable isotopes; quantitative X-ray diffraction.

1. Introduction

Storage of CO_2 in carbonate minerals has been recognized as a safe and effective method for mitigating rising concentrations of atmospheric greenhouse gases (Seifritz, 1990; Lackner et al., 1995; Lackner, 2003). Since carbon mineralization was first proposed as a method for storing CO_2 (Seifritz, 1990), most of the work on this subject has focused on the development of rapid, large-scale *ex situ* methods for trapping and storing CO_2 at industrial point sources (reviewed in Huijgen and Comans, 2003, 2005; IPCC, 2005; Sipilä et al., 2008; Power et al., in review). Most processes developed to date are based on reaction of CO_2 with naturally occurring non-carbonate minerals such as silicates, hydroxides or oxides. Weathering of these minerals in nature is generally a slow process and high temperatures and pressures are needed to induce carbon mineralization reactions on the short timescales (i.e., hours) required for development and deployment of industrial carbonation reactors (Sipilä et al., 2008; Zevenhoven et al. 2011). Although technologically feasible, the financial viability of this approach to carbon mineralization is currently limited by low carbon prices (Power et al., 2013; Power et al., in review). Thus, low-temperature and low-pressure carbonation of alkaline industrial wastes such as smelter slag, fly ash, alkaline and saline brine, construction waste, and mine tailings is an attractive alternative technology (e.g., Wilson et al., 2006, 2009a,b, 2010, 2011; Manning, 2008; Ferrini et al., 2009; Huntzinger et al., 2009; Power et al., 2009, 2010, 2011; Renforth et al., 2009, 2011; Ballirano et al., 2010; Zhao et al., 2010; Pronost et al., 2011, 2012; Bobicki et al., 2012; Harrison et al., 2013; Manning and Renforth 2013). In situ carbonation of the mineral waste from ultramafic mines has been documented previously (Wilson et al., 2006, 2009a,b, 2011; Pronost et al., 2012; Bea et al., 2012; Beinlich and Austrheim, 2012), but systematic measurement and modeling of this phenomenon have not previously been attempted on the scale of a large operating tailings facility.

At the Mount Keith Nickel Mine, Western Australia, the hydrated Mg-carbonate mineral, hydromagnesite [$Mg_5(CO_3)_4(OH)_2{\cdot}4H_2O$], develops as a weathering product within ultramafic mine tailings. Consequently, accounting of the amount of atmospheric CO_2 that is being trapped and stored

within this mineral could be used to offset the mine's greenhouse gas emissions. Accelerating the carbonation of mine tailings at Mount Keith has the potential to completely offset the net greenhouse gas emissions of this mine.

The mineral content of mine tailings is generally heterogeneous due to frequent changes in ore mineralogy, processing procedures, and tailings management practices. The mineralogy of tailings piles also changes with time as tailings react with the atmosphere and meteoric and process waters to produce secondary mineral phases. As a result, geostatistical methods that rely on the presence of regular and predictable geological structures cannot be used to predict the mineralogy of a mine tailings pile. In order to estimate the total amount of CO_2 captured within secondary carbonate mineral phases at a mine, it is necessary that the mineralogy of its tailings storage facilities be well constrained. Using the Rietveld method and powder X-ray diffraction (XRD) data, we have constructed a database of quantitative mineralogical results for a large suite of tailings samples from Mount Keith. Because the ages are known for many of the tailings flows at Mount Keith, we have been able to use our quantitative mineralogical results to build a reactive transport model that describes the geochemical evolution of the tailings storage facilities (Bea et al., 2012; this study). From this model, we illuminate the mechanisms governing carbon mineralization and obtain an empirical rate for hydromagnesite precipitation. The isotope system (i.e., $\delta^{13}C$, $\delta^{18}O$, and $F^{14}C$) employed by Wilson et al. (2009a) has been used to assess trapping of atmospheric CO_2 within hydromagnesite in the tailings at Mount Keith. Finally, the reactive transport model has been used to assess potential methods for enhancing carbon mineralization in tailings.

2. Locality and sampling strategy

2.1. The Mount Keith Nickel Mine

The MKD5 orebody at Mount Keith is located in the North Eastern Goldfields district of Western Australia (Fig. 1) and is the largest nickel producer in Australia (Grguric, 2003). The deposit

at Mount Keith occurs in the NNW/SSE-trending Agnew–Wiluna greenstone belt in the Archaean Yilgarn Craton (Hill et al., 1990). The MKD5 orebody is hosted by komatiitic peridotite (primarily dunite), which attained mid–upper greenschist facies as a result of regional metamorphism (Barrett et al., 1977). Retrograde serpentinization and carbonation of the host peridotites resulted from infiltration by H_2O–CO_2-rich fluids (Barrett et al., 1977; Grguric et al., 2006). Resulting metamorphic assemblages (from proximal to distal) are (1) talc–magnesite, (2) antigorite–magnesite, and (3) lizardite–brucite–hydrotalcite group (Grguric et al., 2006).

Conventional, staged-cutback, open pit mining methods are practiced at MKD5, yielding approximately 11 Mt of ore annually (Grguric, 2003). The mining operation at MKD5 produces approximately 370 000 t of greenhouse gases (cited as CO_2 equivalent) and approximately 11 Mt of ultramafic tailings each year (BHP Billiton, 2005). Ore from the MKD5 deposit is processed using froth flotation methods to concentrate sulfide minerals (Grguric et al., 2006). Additives used in processing include citric and sulfuric acids, guar gum, Na-dithionite, Na-ethyl xanthate, and (historically) soda ash. In 2004, ore reserves contained 0.52 wt.% nickel (Grguric et al., 2006), primarily in high-Ni pentlandite [$(Fe,Ni)_9S_8$], godlevskite [$(Ni,Fe)_9S_8$], heazlewoodite [Ni_3S_2], and millerite [NiS]. Recovery of these minerals from the flotation circuit is typically about 70% (Grguric et al., 2006). The material rejected from the processing plant is piped to one of two tailings storage facilities (TSF2, which was the only facility in operation at the time of sampling), and is suspended in the hypersaline process water used in the flotation circuit. Tailings are deposited from spigots located on risers at nine points in TSF2 (Fig. 1a).

The tailings storage facility at Mount Keith was constructed in two phases. The two cells of TSF1 (Fig. 1a) were the sole receptacles for tailings from July 1994 until the facility was decommissioned in January 1997 (Stolberg, 2005). A centralized discharge tailings storage facility (TSF2) was commissioned to replace TSF1 by January 1997 (Stolberg, 2005) and remains in operation today. Along the circumference of TSF2, the outer 100 to 400 m of the compound are dedicated to

catching and storing tailings in the event that mineral waste from the interior of the facility should overflow. This design feature has been effective and provides snapshots of tailings compositions from several overflow events. Tailings in the various overflow cells of TSF2 have been permitted to weather, without addition of new tailings or process water, for periods of one, three, and between seven and eight years prior to sampling in 2006. At the time of sampling, tailings in the interior of TSF2 (along the radial access road, Fig. 1a) had last been deposited approximately zero or one half years prior to collection.

2.2. Strategy for sampling at Mount Keith

Limited sampling of the tailings storage facilities at Mount Keith was begun in April 2005. More extensive sampling was done in September and October of 2006. In excess of 800 samples were collected from TSF2 and the older, now-decommissioned TSF1. Bea et al. (2012) describe detailed quantitative mineralogical results and reactive transport modeling of TSF1.

At the time of fieldwork, large regions of TSF2 were saturated with process water, making these regions of the tailings facility inaccessible for sampling. In order to compensate for incomplete access to the tailings at Mount Keith, sampling of the main tailings storage facility (TSF2) was carried out along a radial maintenance road and around the perimeter of the roughly circular facility (Fig. 1a). Samples were collected at random intervals along these two paths in TSF2. Tailings were primarily sampled by collection of single cores, coring on 5 m x 5 m and 10 m x 10 m grids (after Roselle et al., 1999) and from vertical profiles on exposed surfaces and excavated trenches. Further detail is available in the Supporting Information.

To the best of our knowledge, all of the tailings (at the surface and at depth) sampled from the overflow cells around the exterior of TSF2 are of a specific age (either one, three, or between seven and eight years). Contrastingly, only the ages of tailings sampled from near the surfaces in the central regions of TSF2 are well constrained (as zero or one half years).

3. Analytical methods

3.1. Qualitative X-ray powder diffraction methods

Qualitative mineralogy was done on selected specimens of efflorescent mineral crusts and microsamples from Mount Keith that were picked with fine tweezers under a binocular microscope. This was done in order to identify sulfate and halide minerals that were present at low abundances within the tailings. Finely ground aliquots of sample were smear-mounted onto petrographic slides with anhydrous ethanol and allowed to dry at room temperature. Powder X-ray diffraction (XRD) data for mineral identification were collected with a scanning step of 0.04° 2θ and counting time of 0.5 s/step on a Siemens (Bruker) D5000 θ–2θ diffractometer equipped with a VÅNTEC-1 detector. The long, fine-focus Co X-ray tube was operated at 35 kV and 40 mA. Mineral phases were identified with reference to the ICDD PDF-4+ database using DIFFRAC^{plus} EVA Version 10.0 (Bruker AXS, 2004a).

3.2. Quantitative X-ray powder diffraction and Rietveld refinement

Quantitative phase analysis with the Rietveld method (Rietveld, 1969; Hill and Howard, 1987; Bish and Howard, 1988) was done on 172 samples of mine tailings from TSF2 at the Mount Keith Nickel Mine. Samples for Rietveld refinement were selected to optimize coverage of the accessible regions of the tailings storage facility. A random number generator was used to select subsets of samples collected from 5 m x 5 m and 10 m x 10 m grids for quantitative phase analysis.

Samples were prepared according to the method of Raudsepp and Pani (2003). XRD data were collected on a Siemens (Bruker) D5000 θ–2θ diffractometer under the same operating conditions used to collect data for qualitative mineralogy. Data for Rietveld refinement were collected with a step size of 0.04° 2θ and counting time of 1s/step over a range of 3–80° 2θ. Rietveld refinements were done with the Topas Version 3 software package (Bruker AXS, 2004b) using the fundamental parameters approach (Cheary and Coelho, 1992). The method of Wilson et al. (2006) was used to compensate for

structural disorder in serpentine-group minerals during refinement. Sources of crystal structure data for detectable mineral phases in the tailings samples, and additional details of the method used for Rietveld refinement, are listed in the Supporting Information.

3.3. Scanning electron microscopy

Mineral habits and the textural relationships amongst minerals were characterized using a Philips XL-30 scanning electron microscope (SEM), equipped with a Princeton Gamma-Tech energy dispersive X-ray spectrometer (EDS) system. Selected samples of tailings were impregnated with epoxy and thin-sectioned for petrographic analysis. Backscattered electron (BSE) imaging was used to observe textural relationships in thin section and EDS was used for the identification of minerals.

3.4. Stable isotopic methods

A total of 100 specimens, taken from 45 geological samples and five samples of water, were analyzed for their stable carbon and oxygen isotopic compositions. Eighteen replicate analyses were done to assess reproducibility of the data. Thirty-two of the specimens of tailings were analyzed in bulk before and after treatment with one normal hydrochloric acid (1 N HCl) at room temperature (i.e., approximately 25ºC). Acid treatment was used to preferentially dissolve hydromagnesite, hydrotalcite-group minerals, and bedrock calcite and dolomite. The untreated specimens reflect the bulk isotopic compositions of all carbonate minerals in the tailings (i.e., bedrock and secondary carbonate minerals), while the acid-treated specimens reflect the isotopic composition of the more resistant bedrock magnesite. Qualitative XRD was done on acid-treated specimens of mine tailings prior to stable isotopic analyses to confirm mineralogy. Stable isotopic data for the resulting 64 specimens, 16 other specimens of mine tailings, and the dissolved inorganic carbon (DIC) in five specimens of water, were collected using standard procedures for stable carbon and oxygen isotopic analyses employed at the Pacific Centre for Isotopic and Geochemical Research (PCIGR), The University of British Columbia.

The stable isotopic compositions of hydromagnesite in 15 specimens of mine tailings were analyzed using selective acid extraction. Detailed isotopic methods are provided in the Supporting Information.

3.5. Radiocarbon procedures

Twenty-three specimens taken from 19 samples were analyzed for ^{14}C content. These comprised one specimen of industrial soda ash, three specimens of highly pure bedrock carbonate minerals, four specimens of CO_2 extracted from magnesite in bulk samples of tailings, and 15 specimens of CO_2 extracted from hydromagnesite in bulk tailings. CO_2 was isolated from magnesite and hydromagnesite in bulk tailings using the method for selective acid extraction described in the Supporting Information. Eight replicate analyses were done to assess reproducibility of radiocarbon data.

Specimens of CO_2 were sealed within glass ampoules at The University of British Columbia and were analyzed for ^{14}C content at the Research School of Earth Sciences at The Australian National University. There, the CO_2 contained within the ampoules was converted to graphite by hydrogen reduction in the presence of iron powder at 550ºC. Graphite targets were placed in a small mould and compressed into pellets. The pellets were run on the Single Stage Accelerator Mass Spectrometer (SSAMS) at The Australian National University. Background contamination, from preparation of graphite targets, was determined from analyses of ^{14}C-free coal and wood and was subtracted from sample data. The Cambridge half-life (5730 ± 40 years) was used to calculate the fraction of modern carbon ($F^{14}C$) as recommended by Donahue et al. (1990) and Reimer et al. (2004). Reservoir corrections were made to $F^{14}C$ values using $\delta^{13}C$ data collected with the SSAMS.

3.6. Reactive transport model description

In order to identify the processes governing hydromagnesite precipitation in the active tailings storage facility at Mount Keith, and to estimate the rate of CO_2 fixation, the reactive transport code

MIN3P (Bea et al., 2012; Mayer et al., 2002) was employed. MIN3P is a multicomponent reactive transport code equipped to simulate transport in variably saturated porous media. It uses the global implicit method, allowing direct coupling between transport and reaction processes (Mayer et al., 2002). Both homogeneous reactions, such as aqueous complexation, and heterogeneous reactions, such as mineral dissolution–precipitation reactions can be modelled. MIN3P was recently modified by Bea et al. (2012) to better represent the influence of dynamic atmospheric conditions on reaction progress by incorporating energy balance equations and vapour transport. Mayer et al. (2002) and Bea et al. (2012) provide complete descriptions of the governing equations and verification examples for MIN3P. MIN3P includes advective–diffusive transport in the aqueous phase, and diffusive gas transport. As such, it is well suited for simulation of carbon mineralization in variably saturated mine tailings.

4. Qualitative mineralogical results and field observations

4.1. Qualitative mineralogy of Mount Keith mine tailings

Tailings at Mount Keith are composed primarily of serpentine minerals, antigorite and lizardite [$Mg_3Si_2O_5(OH)_4$], with hydrotalcite-group minerals including iowaite [$Mg_6Fe^{3+}_2(OH)_{16}Cl_2{\cdot}4H_2O$] and woodallite [$Mg_6Cr_2(OH)_{16}Cl_2{\cdot}4H_2O$] with occasional pyroaurite [$Mg_6Fe^{3+}_2(OH)_{16}CO_3{\cdot}4H_2O$], stichtite [$Mg_6Cr_2(OH)_{16}CO_3{\cdot}4H_2O$], and uncommon mountkeithite [$(Mg,Ni)_{11}(Fe,Cr)_3(OH)_{24}(SO_4,CO_3)_{3.5}{\cdot}11H_2O$]. A solid solution exists between iowaite, woodallite, pyroaurite and stichtite and ideal end-member compositions are generally not observed at Mount Keith (Grguric, 2001). Minor amounts of brucite, chrysotile, talc, magnetite, chromite, quartz, magnesite, dolomite, and calcite are common. Trace vermiculite is also observed in the tailings. Sulfide minerals have not been detected with XRD to a limit of approximately 0.5 wt.%. These observations are consistent with ore mineralogy (Grguric, 2003).

Efflorescences of secondary minerals are abundant near surfaces within the tailings storage facilities and include carbonate minerals, halide minerals and sulfate minerals (listed in SI Tables S1

and S2). Efflorescences of sulfate minerals commonly form at the surface of mine tailings during dry conditions or in arid climates, and are leached from tailings during rainfall events (Jambor et al., 2000). At Mount Keith, hydromagnesite, halite, hexahydrite [$MgSO_4 \cdot 6H_2O$], and blödite [$Na_2Mg(SO_4)_2 \cdot 4H_2O$] dominate these efflorescences, and are commonly associated with lesser amounts of epsomite [$MgSO_4 \cdot 7H_2O$], konyaite [$Na_2Mg(SO_4)_2 \cdot 5H_2O$], löweite [$Na_{12}Mg_7(SO_4)_{13} \cdot 15H_2O$], and gypsum [$CaSO_4 \cdot 2H_2O$]. Sanderite [$MgSO_4 \cdot 2H_2O$], starkeyite [$MgSO_4 \cdot 4H_2O$], pentahydrite [$MgSO_4 \cdot 5H_2O$], and carnallite [$KMgCl_3 \cdot 6H_2O$] are less common and have only been observed at low abundance. Kainite [$Mg(SO_4)KCl \cdot 3H_2O$] and anhydrite [$CaSO_4$] may or may not be present near detection in a very few of the samples analyzed. The hydration states of sulfate minerals are strongly dependent on temperature and relative humidity (e.g., Chou and Seal, 2003, 2007; Chipera and Vaniman, 2007) and double salts are known to decompose to single salts (e.g., konyaite and blödite may decompose to produce thenardite, hexahydrite and amorphous phases; Mills et al., 2010). Thus, the relative abundances of hydrated sulfate minerals measured in the laboratory may not reflect abundance in the field.

4.2. Occurrence of hydromagnesite mineralization

Hydromagnesite was detected by XRD in the majority of samples, but is more commonly found at high abundance in samples of shallow tailings. SEM images of Mount Keith mine tailings commonly show fine crystals of hydromagnesite precipitating at the surface of grains of serpentine (Fig. 2). In some instances, this hydromagnesite infills both fine cracks and broad fissures in serpentine grains (Fig. 2a). The latter textures suggest that hydromagnesite may be forming by replacement of serpentine. Micrometer-scale crystals of hydromagnesite radiate out into the spaces between tailings grains and commonly cement them together (Fig. 2b). These textures are similar to those described by Wilson et al. (2009a) for dense cements of hydromagnesite [$Mg_5(CO_3)_4(OH)_2 \cdot 4H_2O$] and dypingite [$Mg_5(CO_3)_4(OH)_2 \cdot 5H_2O$] that form at depth within tailings at the Clinton Creek chrysotile mine,

Yukon, Canada. The textural relationship between hydromagnesite and gangue minerals such as serpentine confirms the secondary origin of hydromagnesite as a weathering product at Mount Keith.

Secondary hydromagnesite is typically concentrated within and just below efflorescent crusts of sulfate minerals; however, hydromagnesite persists at depth within the tailings at Mount Keith whereas sulfate minerals generally do not. Although tailings that are heavily cemented with hydromagnesite commonly occur near the surface of TSF2, hydromagnesite-rich samples are also encountered at depth within the tailings storage facility.

Excavating trenches within TSF2 to collect profile samples reveals distinct horizons of tailings material. Within these profiles, layers of clay and silt sized tailings commonly overlay layers of sand sized tailings. These well-sorted layers are likely indicative of mass settling within tailings flows during distinct depositional events [see upper 2 m of the profile at sampling site 1 (i.e., 06MKP1 within 0.5-year old tailings)], which is illustrated in Fig. 3a and 3b. Tailings flows consisting of fine and coarse layers range from 1 cm to 40 cm thick. The most recently deposited tailings in 06MKP1 are covered by an efflorescent crust of blödite and halite and are enriched in hydromagnesite (samples labeled 1–3 in Fig. 3a). Hydromagnesite and sulfate minerals are not detectable in the layers of fine sand (4) and coarse sand (5) beneath the surficial samples. However, hydromagnesite is present in deeper samples (6–8) that are associated with filled desiccation cracks (located between samples 7 and 8). Again, hydromagnesite is absent from sample 9, which grades into medium to coarse sand, but it reappears in sample 10. Although sample 10 is of coarse sand, it is a thin horizon and is in contact with a deeper, silty layer (11) that also contains hydromagnesite. The same trend of coarsening grain size with increasing depth occurs between samples 11 and 14, all of which contain hydromagnesite. Filled desiccation cracks appear once again between sample 14 and the fine-grained, hydromagnesite-rich tailings from sample 15. Beneath this level, at a depth of approximately 160 cm, the tailings become darker in color and smell faintly of organics.

Desiccation cracks are a common feature within mine tailings at the surfaces of TSF2. Within weeks to months of tailings deposition, desiccation cracks begin to appear within the upper few centimeters of new tailings flows. Shallow, distantly spaced desiccation cracks can be seen in the newly deposited tailings at sampling site 30 (Fig. 3c). Stolberg (2005) notes that such cracks form within one month in column experiments conducted on water-saturated tailings from Mount Keith when these are left to drain. After approximately 6–12 months, many more cracks will have propagated within the hardened efflorescences on tailings surfaces (Fig. 3d). If the tailings are left exposed for a significant amount of time, the desiccation cracks can become deeper features as efflorescent sulfate minerals are leached from the surficial tailings, leaving behind hardened blocks and layers of hydromagnesite-cemented tailings (Fig. 3e).

The prevalence of desiccation cracks at tailings surfaces, the preservation of infilled desiccation features at depth, and the higher abundance of hydromagnesite within deep samples such as 06MKP1-8 and 06MKP1-15 indicate that the horizons from which they were taken were once exposed at the surface. It is particularly notable that these former surfaces and the horizons adjacent to them are enriched in hydromagnesite compared to the hydromagnesite-poor horizons of tailings that separate them. While hydromagnesite is most abundant near tailings surfaces, observations of hydromagnesite in deep, sandy horizons suggests that it may continue to precipitate or become reworked at depth.

4.3. Consequences of timing and depth of tailings deposition for hydromagnesite formation

Most of the sampling in TSF2 was done to depths between zero and 130 cm using a sediment-coring device. The ~35-meter tall W1 riser (near sampling sites 1 and 2, Fig. 1a) was buried in tailings to a depth of 19 m at the time of sampling. This represents an average deposition of approximately 2 m of tailings each year from the time TSF2 was commissioned up until the time of sampling. However, mine tailings deposits are commonly less than 1 m deep within the exterior overflow cells and at the edges of the large central cell of TSF2. Mining at Mount Keith produces approximately 11 Mt of

tailings each year. If this mass of tailings were deposited uniformly throughout TSF2 it would be approximately 50 cm in depth. After 10 years (i.e., from January 1997 to October 2006) of uniformly thick deposition, tailings deposits would be 5.0 m deep. Clearly, the deep deposits that surround risers are not typical of all regions within TSF2, which suggests that depths on the order of meters are more common than those on the order of decameters.

Stolberg (2005) gives values of 3.0 to 3.8 m for the depth of the tailings deposited near the center of Cell 2 in the now unused TSF1 (i.e., the rightmost cell in Fig. 1a) and values as high as 10 m for the depth of tailings near discharge points along the perimeter of Cell 2. As such, deep grid samples in TSF1 and, similarly, near the risers in TSF2 would most likely be accessing tailings deposited within one year of last deposition at the surface. Following this line of reasoning, we have attributed the same ages known for the surface deposits to the deeper tailings in our analyses.

Mount Keith experiences an average pan evaporation of 2,400 mm/yr and limited rainfall (220 mm/yr on average), most of which is lost to evapotranspiration (Stolberg 2005). The location of the watertable within most regions of TSF2 was difficult to assess by coring; however, the water table was observed at an elevation of 524.3 m above sea level at both sampling site 30 and at the water return pond (sampling site 25). At sampling site 30, samples collected with a backhoe excavator were saturated with water, indicating that they had been collected from beneath the vadose (unsaturated) zone. Recently deposited tailings from some areas of TSF2 were wetted beneath efflorescent crusts, and coring holes through these damp tailings had a tendency to swell shut within minutes of sampling, but standing water was not observed. This suggests that in parts of TSF2, only the upper few meters of tailings are unsaturated.

Darkly colored, anoxic samples were collected from the base of the profile at sampling site 1, from the base of the backhoe trench at sampling site 30 (Fig. 3c) and from shallow depth (i.e., < 20 cm) near the water return pond. These samples may reflect a prevalent compositional change within the deeper, anoxic tailings that are located within the saturated zone of TSF2. Hydromagnesite was present

within the anoxic samples from sites 1 and 30 at abundances comparable to those in the unsaturated zone, suggesting that hydromagnesite is relatively insoluble within the saturated zone of TSF2 and would persist at depth following burial. Thus, estimates of hydromagnesite abundance, made predominantly from samples collected from within the vadose zone, should still apply to deeper, saturated tailings.

5. Analytical results

5.1. Rietveld refinement results

Rietveld refinement results for tailings from Mount Keith are shown in Figs. 4 through 7 and the complete dataset is available in SI Table S5. Refined abundances and median abundances for hydromagnesite are plotted in Fig. 4 for tailings of five different ages (i.e., 0 years, 0.5 years, 1 year, 3 years and 7 to 8 years) Shaded envelopes denote the median plus or minus the median absolute deviation of mineral abundance (e.g., Upton and Cook, 2009) for depth intervals (in cm) of [0, 25), [25,50), [50, 75), [75, 100), [100, 125), [125, 150), and [150, maximum depth]. Data are plotted similarly in Figs. 5 through 7. Results for 10-year old tailings from TSF1 are discussed and modeled by Bea et al. (2012). We use the median and median absolute deviation (MAD) as measures of central tendency because Rietveld refinement results produce a sparse set of log-normally distributed data. Statistical analyses are discussed in more detail in the Supporting Information.

5.2. Stable isotopic results

The $\delta^{13}C$ values for carbonate minerals from Mount Keith mine tailings (see Fig. 8 and SI Table S6) vary from -8.56‰ to +1.04‰ (VPDB), with $\delta^{18}O$ ranging from 7.81‰ to 39.89‰. (VSMOW). One specimen of bedrock magnesite from a sample of wasterock is characterized by $\delta^{13}C_{VPDB}$ = -6.52‰ and $\delta^{18}O_{VSMOW}$ = 7.91‰. A specimen of iowaite (a hydrotalcite-group mineral) from the mine

pit gives values of $\delta^{13}C_{VPDB}$ = -2.83‰ and $\delta^{18}O_{VSMOW}$ = 16.11‰. Specimens of late-stage Ni-dolomite alteration give -6.58‰ ≤ $\delta^{13}C_{VPDB}$ ≤ -5.78‰ and 26.35‰ ≤ $\delta^{18}O_{VSMOW}$ ≤ 27.86‰ ($\delta^{13}C_{av}$ = -6.16‰ and $\delta^{18}O_{av}$ = 27.30‰). Bedrock magnesite, isolated from tailings by selective acid dissolution, gives values of -6.79‰ ≤ $\delta^{13}C_{VPDB}$ ≤ -1.23‰ and 10.33‰ ≤ $\delta^{18}O_{VSMOW}$ ≤ 18.98‰ ($\delta^{13}C_{av}$ = -4.11‰ and $\delta^{18}O_{av}$ = 13.27‰). Notably, magnesite extracted from bulk tailings is slightly more enriched in ^{13}C and significantly enriched in ^{18}O over the specimen of pure magnesite that was sampled from wasterock. Duplicate analyses of one sample of soda ash (used historically as an industrial process chemical) give average values of $\delta^{13}C_{VPDB}$ = -8.69‰ and $\delta^{18}O_{VSMOW}$ = 17.73‰. Dissolved inorganic carbon in tailings water gives values of –8.16‰ ≤ $\delta^{13}C_{VPDB}$ ≤ -6.20‰ ($\delta^{13}C_{av}$ = -7.36‰). Water from the processing plant gives values of -6.91‰ and -4.60‰ ($\delta^{13}C_{av}$ = -5.76‰).

Analyses of bulk carbonate minerals give -6.70‰ ≤ $\delta^{13}C_{VPDB}$ ≤ -0.33‰ and 14.16‰ ≤ $\delta^{18}O_{VSMOW}$ ≤ 31.97‰ ($\delta^{13}C_{av}$ = -3.46‰ and $\delta^{18}O_{av}$ = 22.60‰). Hydromagnesite, isolated by selective acid extraction, is characterized by -8.6‰ ≤ $\delta^{13}C_{VPDB}$ ≤ 1.0‰ and 24.5‰ ≤ $\delta^{18}O_{VSMOW}$ ≤ 39.9‰ ($\delta^{13}C_{av}$ = -3.0‰ and $\delta^{18}O_{av}$ = 34.8‰). On average, secondary hydromagnesite is enriched over magnesite by approximately 1‰ in $\delta^{13}C$ and approximately 22‰ in $\delta^{18}O$.

5.3. Radiocarbon results

The $F^{14}C$ values for carbonate minerals at Mount Keith range from 0.004 to 1.052 and are given in Fig. 9 and SI Table S6. Average values of $F^{14}C$ and $\delta^{13}C_{VPDB}$ are plotted for samples on which replicate analyses have been done. Because $\delta^{13}C$ data for four specimens of magnesite are not available, radiocarbon results are plotted for two of these specimens only (i.e., CO_2 selectively extracted from magnesite in samples 06MKG-2-7-3 and 06MKG10-5-1).

One specimen of bedrock Ni-dolomite gives an $F^{14}C$ of 0.004 and two specimens of highly pure bedrock magnesite are characterized by 0.005 and 0.009 (the latter value is an average of two

analyses). These results for highly pure bedrock carbonate minerals are consistent with ^{14}C-free carbon and the level of atmospheric contamination expected from gas separation in our vacuum line and preparation of graphite samples. Carbon dioxide extracted from magnesite in four bulk samples of tailings is defined by $0.024 \leq F^{14}C \leq 0.365$ ($F^{14}C_{av} = 0.147$), the upper end of this range of values being significantly higher than expected from measurements on highly pure specimens. One specimen of soda ash (used historically as a process chemical in the flotation circuit at Mount Keith) has an $F^{14}C$ of 0.052. Analysis of CO_2 selectively extracted from hydromagnesite is characterized by $0.572 \leq F^{14}C \leq 1.052$ (average $F^{14}C = 0.921$).

6. Discussion of mineralogical and isotopic results

6.1. Mineralogical change and formation of hydromagnesite

6.1.1. Occurrence of efflorescent minerals

The most common and abundant efflorescent phases at Mount Keith are secondary hydromagnesite, sulfate minerals and halite. The distribution of these phases changes with depth below the tailings surface and evolves with time since deposition of tailings in TSF2.

The abundances of both hydromagnesite and halite in tailings of all ages are greatest within 0 to 25 cm of the surface (Figs. 4 and 5). This is consistent with previous observations and model results, which indicate that secondary efflorescent minerals are more likely to form within an evaporative horizon at the contact between tailings and the atmosphere (e.g., Acero et al., 2007, 2009; Bea et al., 2012). The abundance of hydromagnesite becomes relatively constant at depths below 25 cm in tailings of each age. However, high abundances of hydromagnesite are sometimes measured at greater depths (Fig. 4), which may reflect partial preservation of crusts from former tailings surfaces or ongoing precipitation at depth. It is also possible that hydromagnesite from buried crusts is being reworked at depth as the tailings settle under their own weight. Both hydromagnesite and halite may also be remobilized to some extent by water percolating through the tailings (primarily process water in TSF2,

with some influence from meteoric water). Quantitative mineralogical results also show that the mean abundance of hydromagnesite within the upper 25 cm increases with time since deposition of tailings. Thus, hydromagnesite precipitation is an ongoing process in TSF2.

It is notable that hydromagnesite abundance follows a similar trend to that for halite (Fig. 5). The formation of halide crusts within tailings in arid climates is known to result from strong capillary transport of aqueous species toward tailings surfaces (Dold, 2006). As with hydromagnesite, the highest concentrations of halite occur at shallow depths, typically above 25 cm (Fig. 5). Halite is also present at depth within the tailings and is found at low abundances in the vast majority of samples analyzed. This suggests that both halite and hydromagnesite remain saturated within tailings and are therefore relatively stable following burial under fresh tailings. Or it could imply that process water is already near saturation with respect to hydromagnesite prior to deposition of tailings, such that percolation of process waters does not significantly remobilize secondary phases.

Sulfate minerals precipitate in mine tailings as a consequence of oxidative weathering of primary sulfide minerals (e.g., Jambor and Blowes, 1998; Jambor et al., 2000). Blödite, hexahydrite and other sulfate minerals are common at the surface of 0- to 1-year old tailings, but persist only at reduced abundance in a few outlier samples at the surface of 3- and 7–8-year old tailings (Fig. 5). Sulfate minerals are scarce below 10 cm depth and are almost entirely absent below a depth of 25 cm. Gypsum, which is relatively insoluble compared to most sulfate minerals, appears to be the only sulfate phase that persists at depth, but it is uncommon and present only at low abundance (Fig. 5). Bea et al. (2012) demonstrate that sulfate minerals are absent from tailings in the non-operational TSF1 at Mount Keith. Without new input of tailings process water, rainfall events likely leach sulfate minerals from the surface of TSF1 within 10 years of deposition (consistent with observations by Jambor et al., 2000). The presence of sulfate minerals in surface crusts suggests that the older tailings flows around the perimeter of TSF2 may occasionally be exposed to fresh tailings water from the interior region of the storage facility. Additionally, the presence of anoxic, darkly colored tailings at depth within TSF2

suggests that surficial sulfate dissolution may be fueling microbial sulfur reduction in deeper tailings horizons.

Acero et al. (2007, 2009) demonstrate that the formation of efflorescent crusts of sulfate minerals reduces the permeability of mine tailings, which limits gas exchange with the atmosphere (i.e., evaporation, and O_2 and CO_2 diffusion). Thus, formation of efflorescences may be viewed as a self-limiting process that controls the depth to which alteration minerals may extend. Precipitation of carbonate and evaporite minerals, such as hydromagnesite and halite, within tailings pores likely participates in controlling the rate and extent of mineralization.

Previous studies have also shown that efflorescent crusts may trap and concentrate upward diffusing gases such as CO_2 in pore spaces near tailings surfaces (Blowes et al., 1991; Tasse et al., 1997; Agnew and Taylor, 2000). Agnew and Taylor (2000) found that CO_2 concentrations in pore spaces beneath a crust of hydrated Fe-sulfate minerals at the Elura Ag-Pb-Zn Mine near Booroondarra, New South Wales, Australia, were up to 10 times that of atmospheric CO_2. This process only occurs where CO_2 is being generated at depth within tailings as a consequence of biodegradation of underlying organics or dissolution of carbonate minerals during biologically mediated oxidation of sulfide minerals. The undetectable quantities of sulfide minerals and high abundances of carbonate minerals within both fresh and weathered tailings suggest that neither process is significant at Mount Keith. Instead, it is more likely that the ubiquitous cracks and fissures that texture efflorescences allow for limited gas exchange between the deeper tailings and the atmosphere once efflorescences have formed.

6.1.2. Relationship of hydromagnesite to primary gangue minerals

Several gangue minerals including serpentine-group minerals, brucite, hydrotalcite-group minerals, magnesite and dolomite could act as sources of magnesium in hydromagnesite. Dissolution of bedrock carbonate minerals could provide DIC into solution; essentially recycling previously fixed carbon into newly formed hydromagnesite. However, this would not constitute net sequestration of

CO_2 within hydromagnesite, which requires a non-carbonate mineral source for both magnesium and carbon (Wilson et al. 2009a).

Variations in the abundances of mined bedrock calcite, dolomite, magnesite and carbonate-bearing hydrotalcite minerals with depth and time are plotted in Fig. 6, and median values show no consistent trends in their distribution with depth or time. In almost all cases, the abundances of bedrock carbonate minerals stay relatively constant in comparison to results for secondary minerals such as hydromagnesite (Fig. 5), which typically show distinct and predictable behaviors with time and depth. Under the circumneutral pH conditions (i.e., pH of 5 to 8) that dominate within the tailings waters at Mount Keith, dissolution of bedrock carbonate minerals will proceed most readily for calcite, then dolomite, and least readily for magnesite (Palandri and Kharaka, 2004). Hydromagnesite is less resistant to dissolution in acidic solutions than magnesite (Königsberger et al., 1999). Hydromagnesite also dissolves rapidly in 5% acetic acid (Wilson et al., 2009a), an acid that has little effect on calcite, the least resistant of the bedrock carbonate minerals. Therefore, the near-constant abundance of less resistant bedrock carbonate minerals and the increasing abundance of hydromagnesite toward the surface of the tailings is very strong evidence that bedrock carbonate minerals are not being dissolved and remineralized as hydromagnesite in TSF2. Secondary Ca-bearing minerals (i.e., gypsum and anhydrite), which could form as a consequence of calcite (and dolomite) dissolution, are relatively uncommon in the tailings at Mount Keith, particularly when compared to the high abundances of secondary Mg-minerals. Only limited dissolution of calcite may be occurring, which indicates that bedrock carbonate minerals are not a significant source of carbon and magnesium in secondary hydromagnesite.

Weathering of serpentine-group minerals and brucite represents an alternative source of magnesium in TSF2. The compositional data for these minerals display a consistent trend toward decreasing abundance with proximity to tailings surfaces (Fig. 7). Abundances of brucite and serpentine minerals are relatively constant below a depth of approximately 25 cm in tailings aged 0 to

7–8 years, but decline rapidly within the upper 25 cm of the tailings. The decrease is coincident with increasing abundance of hydromagnesite. This effect is particularly marked for brucite, for which the median abundance and MAD decline to 0 wt.% for all surficial tailings aged 0 to 7–8 years. Contrastingly, brucite is typically present at 1.0–2.5 wt.% abundance throughout the deeper, less weathered samples from TSF2.

Median values for the abundance of serpentine decline by approximately 10 wt.% over the depth interval from 25 cm to 0 cm. This is, however, a proportionally minor decrease in the abundant serpentine minerals when compared to the complete loss of brucite. Bea et al. (2012) have shown that such trends can be caused by dilution of primary gangue minerals as secondary minerals precipitate from tailings water, solutes and atmospheric gases. Significant input of new crystalline mass to previously unaltered tailings results in a dilution effect in mineral abundances. This occurs because Rietveld refinement results provide a relative measure of crystalline mass, normalized to 100% (w/w).

Weathering of brucite is known to produce hydromagnesite and other hydrated Mg-carbonate minerals under conditions of temperature and pressure that prevail at the Earth's surface (e.g., Hostetler et al. 1966; Xiong and Lord 2008). Recent carbonation experiments (e.g., Wilson et al., 2010; Zhao et al., 2010; Hövelmann et al., 2012; Harrison et al., 2013) indicate that brucite carbonation can be rapid at near-ambient pressures and temperatures, even in saline and alkaline brines similar to the tailings water at Mount Keith (Wilson et al., 2010; Harrison et al., 2013). Bea et al. (2012) and Beinlich and Austrheim (2012) have also documented brucite carbonation in mine tailings from TSF1 at Mount Keith and in a sub-arctic mine shaft, respectively. Interestingly, no brucite was observed during SEM imaging of hydromagnesite-rich surface samples, which is consistent with the brucite abundance decreasing to 0 wt.% near tailings surfaces in TSF2. Grguric (2003) describes a common texture within Mount Keith ore whereby brucite forms coronas with magnetite that encompass sulfide blebs. Thus, the absence of brucite is explained by the (otherwise perplexing) overgrowths of hydromagnesite on magnetite grains (observed in Fig. 3b). This textural feature may play a role in limiting sulfide

oxidation and carbonate mineral dissolution within Mount Keith tailings. Textural evidence from SEM imaging of particularly hydromagnesite-rich samples (Fig. 3a and b) also shows platy hydromagnesite crystals seeding from grains of serpentine minerals, which is consistent with serpentine carbonation. Carbonation of serpentine-group minerals in alkaline mine tailings is known to produce similar textures in brucite-free mine tailings (Wilson et al., 2009a). These results imply that the observed decreases in the abundances of both serpentine and brucite are very likely the result of two processes: (1) dissolution to produce secondary Mg-bearing minerals such as hydromagnesite, and (2) a dilution effect caused by incorporation of water and atmospheric gases into these newly formed minerals.

6.2. Carbon reservoir fingerprinting

There are four potential sources of carbon in tailings from operating mines like Mount Keith: (1) atmospheric CO_2, (2) bedrock carbon from gangue carbonate minerals, (3) carbon from industrial additives, and (4) organic carbon (i.e., mine camp sewage, mined organic sediments, decay of local biota, or microbial metabolism). Net sequestration of CO_2 requires that there be a non-carbonate mineral source for cations and carbon. Thus, net sequestration of CO_2 can only occur in mine tailings when atmospheric carbon (either directly from the atmosphere or indirectly from modern organic matter) is fixed within the crystal structures of carbonate minerals. XRD techniques are well suited to identifying and quantifying carbonate minerals, but these techniques cannot discern which minerals are trapping and storing atmospheric CO_2 nor to what extent CO_2 is being sequestered. Stable and radiogenic carbon and stable oxygen isotope data can be used to: (1) identify the sources for CO_2 stored in carbonate minerals, (2) elucidate the mechanisms by which minerals form, and (3) trace the processes by which carbon is cycled.

6.2.1. Fingerprinting with stable isotopes

Values for $\delta^{13}C_{VPDB}$ between -10‰ and +1‰ with $\delta^{18}O_{VSMOW}$ in the range of approximately 10‰ to 20‰ commonly reflect the isotopic compositions of metamorphic magnesite (e.g., Kralik et al., 1989; Hansen, 2005). The majority of the stable isotopic data for magnesite fall within this range of values (Fig. 8) and are consistent with a metamorphic origin for this mineral at Mount Keith. One specimen of a hydrotalcite-group mineral (carbonate-bearing iowaite) has a similar stable isotopic signature to the specimens of magnesite. Specimens of Ni-dolomite are also similarly depleted in ^{13}C, but are significantly enriched in ^{18}O relative to the other bedrock carbonate minerals. This is consistent with their origin as fracture coatings and vug linings in oxidized ore (Grguric, 2003). Soda ash, which was used historically as a process chemical, is slightly depleted in ^{13}C relative to bedrock carbonate minerals and gives $\delta^{18}O$ values that are comparable to the upper range for specimens of magnesite.

Samples of bulk carbonate in mine tailings are consistently enriched in ^{18}O relative to bedrock magnesite and many are enriched relative to Ni-dolomite. Analyses of hydromagnesite, done using selective acid extraction, indicate further enrichment in ^{18}O (with some $\delta^{18}O_{VSMOW}$ values reaching 40‰) accompanied by a small enrichment in ^{13}C of ~1‰ on average. The significant enrichment of ^{18}O in hydromagnesite relative to magnesite suggests precipitation in an evaporative environment. This is consistent with our interpretation that hydromagnesite forms as a secondary alteration mineral.

Neither the equilibrium carbon isotopic fractionation factor for hydromagnesite–CO_2 nor for hydromagnesite–HCO_3^- is known; however, the fractionation factor for dypingite [$Mg_5(CO_3)_4(OH)_2 \cdot 5H_2O$], a structurally and chemically related mineral, has been estimated to be $10^3 \ln\alpha_{dypingite–HCO3-} = (3.8 \pm 1.2)$‰ between 20˚C and 25˚C (Wilson et al., 2010). Therefore, we have used the fractionation factor for dypingite to define fields for precipitation of hydromagnesite in equilibrium with atmospheric CO_2 ($-9‰ \leq \delta^{13}C_{VPDB} \leq -7‰$) and DIC in tailings water (Figures 8 and 9). The temperature dependence of the fractionation factor of dypingite is not known; however, values

for equilibrium precipitation of carbonate minerals are known to increase in value with decreasing temperature and vice versa (Chacko et al., 2001). Thus, the anticipated range of $\delta^{13}C$ values is expected to be broader than shown owing to seasonal temperature variations at Mount Keith. The lower limit to $\delta^{18}O$ in the fields for equilibrium precipitation of hydromagnesite from both atmospheric CO_2 and tailings water DIC is defined by the equilibrium oxygen isotopic fractionation factor for hydromagnesite reported by O'Neil and Barnes (1971) at 25˚C, $10^3 ln\alpha_{hydromagnesite–H2O} = 31.2‰$, and assuming tailings process water, derived from local groundwater, has a minimum value of $\delta^{18}O_{VSMOW} \approx -7‰$. This value reflects the lower range of monthly rainwater data for Perth, which is the only Western Australian sampling site in the Global Network of Isotopes in Precipitation (IAEA/WMO, 2012).

Oxidized sewage organic matter may act as a source of carbon for carbonate mineral precipitation in mine tailings (Wilson et al., 2011). Thus, the processed mine camp sewage that is disposed of within TSF2 could reflect another possible source of carbon. The field marked "organic" in Fig. 8 indicates the predicted $\delta^{13}C$ composition of carbonate minerals precipitated from sewage (defined by values derived from Burnett and Schaeffer, 1980; Spies et al., 1989; Gearing et al., 1991; Van Dover et al., 1992; Bachtiar et al., 1996; deBruyn and Rasmussen, 2002; Fernandes et al., 2005; Ramírez-Álvarez et al., 2007).

None of the data for hydromagnesite at Mount Keith fall within the fields defined for mineral precipitation in equilibrium with atmospheric CO_2 or mine camp sewage. However, most of the data for hydromagnesite are consistent with precipitation in equilibrium with DIC in process/tailings water at approximately 25˚C. Based on comparison with carbon isotopic fractionation factors between other carbonate minerals and DIC, it is likely that inclusion of temperature dependence for dypingite-DIC fractionation (Wilson et al., 2010) would increase the breadth of this field to include all the remaining data for hydromagnesite. Although results are consistent with precipitation of hydromagnesite in equilibrium with process water and DIC, the ultimate source of carbon in DIC is not apparent from

stable isotope data. Process water DIC and tailings water DIC at Mount Keith (-8.16‰ ≤ $\delta^{13}C_{VPDB}$ ≤ -4.60‰) are consistently depleted in ^{13}C relative to DIC in equilibrium with the atmosphere (i.e., $\delta^{13}C_{VPDB}$ ≈ 0‰ at 25˚C). The observed carbon isotopic signature of DIC in process and tailings water may reflect (1) kinetic depletion of ^{13}C during diffusion of atmospheric CO_2 into solution (i.e., O'Neil and Barnes, 1971; Wilson et al., 2010; Harrison et al., 2013), (2) input of organic or soil CO_2 into the tailings waters, (3) the use of ^{13}C-depleted chemicals during processing, or (4) dissolution of ^{13}C-depleted bedrock carbonate minerals.

6.2.2. Fingerprinting with radiocarbon

$F^{14}C$ values for CO_2 selectively extracted from hydromagnesite range from 0.572 to 1.052 and all but one specimen has $F^{14}C > 0.8$ (Fig. 9). A value of $F^{14}C = 1.06$ reflects the ^{14}C concentration of the atmosphere in 2006, the year of sampling at Mount Keith (Levin et al., 2008). Thus, the highest values in this range are consistent with a modern source for approximately 100% of the DIC-derived carbon in hydromagnesite. The average $F^{14}C$ value of hydromagnesite is $F^{14}C_{av} = 0.921 \pm 0.145$, which suggests that, on average, at least 87% of carbon in these samples has a modern source. The only known large reservoir for modern carbon at Mount Keith is the atmosphere and, based on our radiocarbon results, it can be concluded that almost all CO_2 mineralized as hydromagnesite originated from this source.

It is important to note that the excursion of some of these data below a $F^{14}C$ of unity suggests the possibility of: (1) partial dissolution and reprecipitation of bedrock carbonate minerals as hydromagnesite, (2) mixing with carbon-bearing process additives during mineral precipitation, or (3) contamination of CO_2 from modern hydromagnesite with CO_2 from ^{14}C-free magnesite during selective acid extraction.

The very small amount of ^{14}C measured in Ni-dolomite sample 06MKNi-dol ($F^{14}C = 0.004$) is consistent with the amount of atmospheric contamination typically observed in our vacuum line for

samples of ^{14}C-free bedrock carbonate minerals. The sample of soda ash has $F^{14}C = 0.052$, which could reflect sourcing of this process additive from a Quaternary evaporite deposit (Warren, 2006). Six specimens of magnesite give values of $0.005 \leq F^{14}C \leq 0.365$. Two of these analyses are of highly pure samples of magnesite found in wasterock at sampling sites 53 and 54 (i.e., 06MK53 and 06MK54), which give $F^{14}C$ values between 0.005 and 0.009. These values are consistent with vacuum line contamination of samples with $F^{14}C = 0$, as expected of bedrock magnesite that formed by carbonate alteration of serpentinized komatiite (Barrett et al., 1977; Grguric et al., 2006). The remaining analyses were done on CO_2 selectively extracted from magnesite in four samples of hydromagnesite-bearing tailings (06MKG2-6-3-mags, 06MKG2-7-3-mags, 06MKG10-5-1-mags, and 06MKP9-4-mags). Magnesite in these samples gives $F^{14}C$ values between 0.024 and 0.365. These values are higher than expected for bedrock magnesite at Mount Keith, which should not contain detectable ^{14}C. Similarly to the few anomalously low $F^{14}C$ values for hydromagnesite, this deviation toward enrichment in ^{14}C within magnesite could reflect (1) partial conversion of secondary hydromagnesite to magnesite or (2) contamination of CO_2 from ^{14}C-free magnesite with modern CO_2 from residual, unreacted hydromagnesite during acid extraction.

The decomposition of hydromagnesite to magnesite has been observed in hydromagnesite playas on the Cariboo Plateau, interior British Columbia, Canada (e.g., Renaut and Long, 1989; Renaut, 1990; Renaut and Stead, 1991). Hydromagnesite represents the dominant mineral phase in these modern lacustrine environments, but magnesite is observed at the surface of the playas during the summer months and may be a product of the decomposition of hydromagnesite. Zhang et al. (2000) estimate that the conversion of hydromagnesite to magnesite requires tens to hundreds of years. However, it may be possible that some amount of recently precipitated hydromagnesite may undergo a transformation to magnesite in the mine tailings at Mount Keith. In fact, the specimen of magnesite with the highest $F^{14}C$ value (i.e., 06MKG10-5-1-mags with $F^{14}C=0.365$) comes from the 10-year old

surface of TSF1. In this case, the mixing trend for magnesite in Fig. 9 could result from precipitation of hydromagnesite and its decomposition to magnesite.

Alternatively, the finely intergrown nature of secondary hydromagnesite (i.e., as a cement between grains of primary tailings minerals) may be preventing complete reaction with phosphoric acid during sample processing. Subsequent processing of these samples at higher temperature and for a longer period of time would then dissolve not only the desired magnesite but also the residual, unreacted hydromagnesite. This would result in higher values of $F^{14}C$ than anticipated for magnesite. Furthermore, the finest fractions of less acid resistant bedrock carbonate minerals such as calcite, dolomite, and hydrotalcite-group minerals may be reacting to some extent during extraction of CO_2 from hydromagnesite. This would produce a dilution in ^{14}C, resulting in artificially low values of $F^{14}C$ for hydromagnesite and the incipient mixing trend in Fig. 9. Thus, we interpret this trend as an artifact of the technique used for sample preparation, which suggests that some $F^{14}C$ values obtained for hydromagnesite are underestimated.

These observations are consistent with the results of previous isotopic studies, which conclude that dissolution of bedrock carbonate minerals does not contribute significantly to production of secondary Mg-carbonate minerals in neutral to alkaline mining environments (e.g., Wilson et al., 2009a, 2011; Beinlich and Austrheim, 2012). Importantly, our radiocarbon results indicate that stable isotope data for Mount Keith carbonate minerals cannot be used to uniquely identify the source of carbon in hydromagnesite. Although radiocarbon data clearly identify a predominantly atmospheric source for carbon, $\delta^{13}C$ data indicate only that hydromagnesite is precipitating in equilibrium with DIC, but out of equilibrium with atmospheric CO_2 gas. Experiments by Wilson et al. (2010) and Harrison et al. (2013) demonstrate that kinetic depletion of ^{13}C occurs during dissolution of atmospheric CO_2 and hydroxylation of aqueous CO_2 to form bicarbonate in saline and moderately alkaline (pH < 11) solutions designed to emulate tailings water at Mount Keith. Mg-carbonate minerals that form from such carbon-limited solutions precipitate in isotopic equilibrium with ^{13}C-depleted DIC (Figs. 8 and 9).

Thus, although hydromagnesite at Mount Keith acts as a store for atmospheric CO_2, this is not immediately apparent due to the impact of diffusion on the $\delta^{13}C$ values of DIC.

7. Reactive transport modeling of hydromagnesite formation in TSF2

7.1. Reactive transport model description and initial conditions

Field observations suggest that formation of hydromagnesite is promoted by evaporation and proceeds primarily within the upper 25 cm of tailings. As such, an atmospheric boundary condition was employed at the surface of a 2.0 m deep × 1.0 m^2 section of tailings to capture the effects of evaporation. Bea et al. (2012) modeled the inactive TSF1 at Mount Keith using atmospheric parameters from a nearby weather station in combination with sinusoidal functions to represent seasonal fluctuations of relative humidity and temperature; the same approach was used in this study. Temperature and relative humidity varied between 11 and 37°C, and 19% and 68%, respectively. Rainfall events were applied to the tailings surface, in accordance with weather data recorded at a nearby weather station (Leinster Airport) in 2010, as short duration events that were repeated annually (after Bea et al., 2012; data from the Australian Government Bureau of Meteorology). Because the atmosphere was deemed to have the most significant influence on the energy balance, a zero energy flux condition was applied at the base of the tailings. A constant head boundary condition (pressure head = 0.0 m) was applied at the base of the tailings to simulate a water table depth at 2.0 mbgs, as is consistent with field observations. Tailings at Mount Keith are deposited as a ~50% slurry of solids and water by mass; therefore, the model domain was initially saturated. All simulations involved 1-dimensional vertical flow only, as is justified by the low hydraulic conductivity of the fine-grained tailings and low horizontal head gradients, which would cause flow to be primarily vertical.

The initial mineralogical composition utilized in the model was based on the afore-described quantitative mineralogical results. Although field observations can only provide snapshots representing the cumulative effects of burial and atmospheric exposure, quantitative mineralogical data indicated

that the abundances of primary mineral phases remain relatively constant through time; therefore, initial abundances were set to values representative of all profiles (SI Table S7). Primary minerals included in the simulations comprised: serpentine (chrysotile), brucite, magnesite, calcite, and dolomite (SI Table S7). An initial value of 2.5 wt.% brucite was estimated based on its average abundance at depth within TSF2, where it presumably was exposed to the atmosphere for a shorter duration, thereby limiting the extent of its dissolution prior to sampling. Hydrotalcite-group minerals were not included in the simulations owing to the lack of data regarding dissolution rates, and the relatively minor abundance of these phases in tailings. Secondary phases that were allowed to precipitate included: hydromagnesite, halite, chalcedony, gypsum, blödite, epsomite, hexahydrite, and nesquehonite (SI Table S7).

Dissolution and precipitation of the primary mineral phases were simulated as kinetically controlled reactions. A far from equilibrium dissolution rate law for chrysotile, a serpentine polymorph, from Thom et al. (2013), was used to describe bulk serpentine dissolution. Although the rate and pH dependence of dissolution for lizardite, antigorite, and chrysotile could differ, the Thom et al. (2013) rate law was used successfully by Bea et al. (2012) to reproduce the observed abundance of serpentine in the inactive TSF1 at Mount Keith. Serpentine dissolution was considered an irreversible reaction whereas brucite dissolution was considered reversible, occurring at a pH-dependent rate prescribed by Pokrovsky and Schott (2004). All other primary phases (calcite, dolomite, and magnesite), were allowed to dissolve only. This is justified by the field-derived mineralogical and isotopic data, which indicate that these phases do not precipitate in the tailings. Moreover, precipitation of magnesite and dolomite is kinetically inhibited at low temperature (e.g., Hänchen et al., 2008; Kenward et al., 2009), and aragonite precipitation is likely to be favored over calcite due to the high Mg:Ca ratio of the process waters (e.g., de Choudens-Sánchez and González, 2009). The kinetic dissolution rate laws and estimated reactive surface areas for primary phases are summarized in SI Table S7. Precipitation of secondary minerals was simulated as a quasi-equilibrium process.

Results from Bea et al. (2012) suggest that atmospheric CO_2 does not ingress past ~50 cm depth in TSF1 at Mount Keith. Yet, hydromagnesite was detected at reasonably high abundance at depths >50 cm in TSF2 (e.g., up to 4.1 wt.% in deep samples collected from 7.5 year old tailings profiles). As described previously, two distinct processes may be invoked to explain the occurrence of hydromagnesite at depth. First, both vertical and lateral fluxes of fresh process water may provide a source of DIC at depth, promoting further precipitation of hydromagnesite after burial. Second, the hydromagnesite within deep tailings samples may have precipitated at the surface when the tailings were first deposited and has persisted at depth following burial under fresh tailings. The plausibility and relative importance of each of these two mechanisms was examined using MIN3P.

In order to estimate the abundance of hydromagnesite that could be derived from process water alone, no hydromagnesite was initially present at depth for simulation of the process water replenishment hypothesis. An average tailings deposition rate of 50 cm/yr was estimated based on 11 Mt/yr of tailings deposited evenly over the ~16.6 km^2 area of TSF2. Field observations of excavated profiles (Fig. 3) indicate that tailings flows are ~10 cm thick on average, suggesting that there are five flows per year that are exposed at the surface for an average of ~70 days prior to burial. One-year long simulations of tailings containing no initial hydromagnesite suggest an average of ~1.95 wt.% hydromagnesite could form within 70 days in the upper 10 cm of the tailings. As such, to simulate the hydromagnesite burial hypothesis, an initial hydromagnesite content of 1.95 wt.% was assigned for depths >50 cm to account for historical hydromagnesite formation during tailings deposition, and in the upper 10 cm, hydromagnesite abundance was set to decline linearly from 1.95 wt.% to 0.00 wt.%. The initial mineralogical composition employed in all simulations is summarized in the Supporting Information.

The initial chemistry of the pore water and fresh process water was set to represent the process water chemistry as indicated by Stolberg (2005) and Bea et al. (2012); it was relatively alkaline (pH = 8.85) and highly saline ($[Na^+]$ = 0.8 M; see Supporting Information). Process water DIC was initially

constrained to be in equilibrium with atmospheric pCO_2 (≈3.45 × 10^{-4} atm), and was therefore initially out of equilibrium with the tailings minerals. The upper boundary solution (i.e., rainfall) chemistry was equal to meteoric water composition at equilibrium with atmospheric pCO_2 (after Bea et al., 2012; see Supporting Information). All solutions were in equilibrium with atmospheric pO_2 (0.21 atm).

Because the simulations were 1-dimensional, a horizontal flux for process water replenishment could not be applied. Therefore, recharge of process water was represented by a constant influx of water spread equally throughout the model domain with vertical flow only. Because flow is dominantly vertical in the unsaturated zone, where it is influenced primarily by gravity and evaporation, a horizontal process water flux is only expected within the saturated zone. Thus, horizontal flow would occur only for fresh tailings that have not yet drained, as well as tailings at depth within the saturated zone. Thus, although the application of a constant flux throughout the upper 2 m of the tailings is a physically improbable scenario, it allowed assessment of the maximum possible extent to which introduction of DIC at depth may affect carbon mineralization, for a given rate of process water recharge. The physical parameters used in the simulations are summarized in the Supporting Information.

Stolberg (2005) measured the vertical hydraulic conductivity of two TSF2 tailings samples, which provided an average saturated hydraulic conductivity (K_{sat}) of 4.88 × 10^{-8} m/s. This K_{sat} value was used for all simulations without process water replenishment (SI Table S9). Stolberg (2005) noted, however, that the horizontal hydraulic conductivity could be 10–100 fold greater than the vertical conductivity. This is due to the manner of tailings deposition, which creates horizontal layers of distinct grain size (Fig. 3) that lead to higher conductivity in coarse-grained layers. This magnitude of anisotropy is consistent with that estimated for other base metal tailings (Yanful et al., 1992). Consequently, a hydraulic conductivity of 4.88 × 10^{-6} m/s was used for the process water replenishment simulation in order to model the maximum lateral process water flux that could be expected in TSF2 (SI Table S9). Assuming any lateral process water flux is primarily driven by the change in elevation

(~14–16 m) across the 4600-meter diameter storage facility, the maximum process water flux at this horizontal K_{sat} is 1.7×10^{-8} m/s, or 3.4×10^{-8} m^3/s through the model domain (2 m^2 cross section). This flux was divided equally throughout the model domain for the process water replenishment simulation, with a constant chemical composition equal to the initial process water composition. The potential effects of reactions occurring up-gradient of the model domain on cation and DIC concentration are neglected, therefore these simulations represent the maximum DIC flux that would be possible. No replenishment of process water was applied to model the hydromagnesite burial hypothesis.

7.2. Reactive transport modeling results and discussion

7.2.1. Mineral dissolution and hydromagnesite precipitation rates

In all simulations, the majority of hydromagnesite precipitation is predicted to occur within the top 25 cm of the tailings, owing to the evapoconcentration of solutes (e.g., Mg^{2+}), dissolution of primary minerals, and the ingress and dissolution of atmospheric CO_2 (Fig. 4), as is consistent with field data. Simulated aqueous magnesium concentrations reach up to 1.0 M at the tailings surface after 7.5 years, which is a tenfold increase over the initial concentration. CO_2 dissolution results in a pH decline near the tailings surface and drives brucite dissolution, leading to the development of a brucite-depleted zone in the near-surface tailings. Mass balance calculations indicate that ~87% of magnesium contained in hydromagnesite is sourced from brucite dissolution, with the balance from magnesium initially present in the pore water. This implies that modest carbon mineralization may still derive from the Mg-rich waters alone, even once the supply of brucite is exhausted, but would be limited by the rate of replenishment of Mg-rich water. The model predicts no serpentine dissolution, as supersaturated conditions existed throughout the tailings pile in the simulations. Textures observed in field samples, however, indicate that a small percentage of the serpentine is carbonated. Passive serpentine carbonation has also been documented in chrysotile and kimberlite-hosted diamond mine tailings that lack brucite (Wilson et al. 2006, 2009a,b, 2011).

A possible explanation for the discrepancy is that there are microenvironments differing in chemistry from the bulk solution that are not captured by the model. For instance, local sulfide oxidation in the near surface could generate acidity, and promote chrysotile dissolution. In addition, there may be complexation effects with organic process water additives that are not adequately accounted for in the model; increased complexation of aqueous magnesium would promote serpentine dissolution. As mentioned previously, the formation of hardpans of efflorescent minerals could also lead to the development of regions with locally elevated pCO_2, by inhibiting gas transport, although this would only occur if CO_2 were generated at depth (e.g., Blowes et al. 1991). Nevertheless, brucite dissolution is sufficient to account for the abundance of hydromagnesite observed (Fig. 4), suggesting that brucite is the primary source of magnesium for carbon mineralization. This is consistent with experimental evidence for the carbonation of brucite in chrysotile mining residues, which demonstrates much greater reactivity of brucite compared to that of chrysotile (Pronost et al., 2011; Assima et al., 2013).

The model predicts relatively rapid brucite dissolution in the near surface environment, with brucite completely removed within ~170 days in the upper 2 cm of the tailings. Correspondingly, ~4 wt.% hydromagnesite is predicted to form within this horizon during this time. With an estimated exposure time of ~70 days at the surface, brucite dissolution at this rate would result in incomplete consumption of brucite prior to burial, leaving up to ~45% of the brucite unreacted (i.e., ~1.1 wt.% remaining), which is consistent with field observations (Figs. 4 and 10).

The brucite dissolution rates were calibrated to mimic those observed for reaction of brucite with CO_2 in air in slurry reactor experiments conducted by Harrison et al. (2013), which was achieved by adjusting the effective surface area of brucite in the model. However, it is likely that the instantaneous brucite dissolution and hydromagnesite precipitation rates calculated by the model are overestimated in comparison to actual reaction rates in the field. This is because the exposure and accessibility of brucite surfaces to CO_2 would likely be lower in tailings than in a continuously stirred

batch reactor owing to unequal porewater distribution and possible surface passivation effects. Precipitation of secondary hydromagnesite at the surfaces of brucite grains may decrease their reactivity, as has been documented for oxide and carbonate coatings that form on pyrite in mine tailings and granular iron in permeable reactive barriers, respectively (Jeen et al., 2006; Nicholson et al., 1989). This effect is not explicitly accounted for in the model.

Although the quantitative mineralogical and isotopic data do not provide adequate temporal and spatial resolution to precisely constrain the instantaneous rate of brucite dissolution, the average annual rates are in good agreement with field observations. An average hydromagnesite precipitation rate for the upper 10 cm of tailings of ~4 wt.%/yr is estimated for TSF2 based on quantitative mineralogical data and modeling results. This corresponds to a CO_2 sequestration rate of ~39 800 t CO_2/yr in the upper 10 cm of tailings, or ~11% of annual mine emissions.

7.2.2. Occurrence of hydromagnesite at depth

Based on agreement with mineralogical data, the modeling results indicate that the presence of hydromagnesite at depth is more likely attributable to burial and reworking of material originally precipitated near the tailings surface as opposed to introduction of fresh DIC in replenished process water (Fig. 4).

The modeled influx of replenished process water, containing atmosphere-equilibrated DIC, is able to drive formation of hydromagnesite at depth without invoking the transport of CO_2 directly from the atmosphere. However, the rate of precipitation is insufficient to explain the observed abundance of hydromagnesite at Mount Keith (Fig. 4). A two-fold increase in DIC flux provided by process waters would be necessary to produce observed abundances of hydromagnesite. This is only possible by having either (1) a higher DIC content in the process water than has been observed at Mount Keith or (2) a two-fold increase in the flux of water to the tailings in TSF2.

There is no evidence to suggest that the initial influx of process water has an elevated DIC content relative to tailings waters. Moreover, even if the process water flux were doubled, the concentration of DIC initially present in the process water would become progressively depleted along the flow path as a consequence of hydromagnesite precipitation. This suggests that, except in the case of tailings located immediately adjacent to risers, the modeled DIC concentrations in the process water supplied to deep tailings likely substantially overestimated the actual DIC concentrations in TSF2. Tailings that are down-gradient along the flow path would receive little DIC in process waters to drive hydromagnesite precipitation, suggesting the modeled amount of hydromagnesite precipitation in these simulations is overestimated. Field measurements of DIC at depth would provide better constraint as to whether DIC is replenished and available for precipitation of hydromagnesite; but tailings pore waters were generally inaccessible at the time of sampling owing to the depth of the water table below the surface of TSF2.

Therefore, it is more likely that the majority of the hydromagnesite documented at depth within TSF2 was initially precipitated near the tailings surface, but has become reworked upon burial. On the scale of the entire tailings impoundment, only negligible precipitation of hydromagnesite may occur due to lateral recharge of DIC-rich process water. Process water DIC may only play a role in hydromagnesite production near risers in the interior of TSF2, where tailings flows are thicker and fresh tailings are generally only exposed to the atmosphere for short periods. Recharge of process water DIC is less likely toward the edges of TSF2; however, the thin tailings flows deposited far from the risers provide an ideal environment for hydromagnesite precipitation via ingress of atmospheric CO_2.

Modeling also predicts that tailings waters may become temporarily undersaturated with respect to hydromagnesite following rainfall events, which could lead to dissolution and redistribution of this phase at depth. Thus, a geochemical mechanism exists by which hydromagnesite may become reworked and more homogeneously distributed within tailings due to transient dissolution of hydromagnesite in near-surface tailings.

8. Potential for accelerating carbon mineralization

Quantitative mineralogical results, microscopy and all simulations suggest that the majority of carbon fixation at Mount Keith occurs via carbonation of brucite. As such, the total mass of hydromagnesite precipitated is largely governed by the brucite content of the tailings and the rate of brucite dissolution. Brucite carbonation is primarily driven by the ingress of atmospheric CO_2 into tailings water. Our stable carbon isotopic data indicate that the rate of CO_2 ingress into Mount Keith tailings water is limited by the slow kinetics of diffusion and dissolution of atmospheric CO_2 into saline, moderately high pH waters (i.e., pH < 11). Therefore, increasing the exposure of tailings waters and brucite to CO_2 has the potential to significantly enhance carbon mineralization rates.

Enhanced carbonation of brucite alone could substantially improve the extent of CO_2 emissions offsetting at Mount Keith. Improving the efficiency of brucite carbonation, to ensure that all the brucite deposited annually within TSF2 were carbonated, would offset the mine's emissions by ~20–60% (Harrison et al. 2013). There are several potential options to achieve this.

8.1. Tailoring tailings deposition rates to enhance reaction with atmospheric CO_2

Passive weathering and carbonation of Mount Keith tailings (i.e., the natural uptake of atmospheric CO_2, which is already occurring) may be facilitated by altering tailings management practices so that reactive phases such as brucite remain near the tailings surface for a longer period of time. For instance, the duration of deposition from individual risers could be decreased, without changing the overall deposition rate, to extend the duration of exposure of fresh, brucite-rich tailings to the atmosphere prior to burial. This might be accomplished by installing a greater number of risers to distribute thinner, more uniform flows of tailings over the entire surface area of TSF2, which is not currently achieved by the small number of risers concentrated in the interior of the facility. Model calculations suggest that at the average rate of tailings deposition at Mount Keith (i.e., ~50 cm/yr), approximately 45% of the initial abundance of brucite remains un-carbonated after burial (Fig. 10),

which is consistent with quantitative mineralogical results. Adoption of a tailings deposition rate of 25 cm/yr would allow more than 80% of the brucite to be carbonated prior to burial (Fig. 10). Decreasing overall rates of tailings deposition may not be feasible at existing mines, as this would require ore processing rates to be lowered. Deposition of tailings over a larger area could achieve the same effect, and thus the footprint of tailings storage facilities could be an important design consideration in the development of prospective mines with ultramafic tailings.

8.2. Direct injection and circulation of CO_2-rich gas streams and DIC-charged waters

Another option for augmenting carbon fixation rates is to circulate air, or CO_2-rich solutions or gases through tailings storage facilities. For example, Harrison et al. (2013) reported a ~240-fold increase in brucite carbonation rates in slurry reactors when the concentration of CO_2 was increased from atmospheric levels (~0.04% CO_2) to 10%. The CO_2 concentration used in these experiments is comparable to that of power plant flue gas (~10–20% CO_2; Kikkinedes, et al. 1993; Uibu et al., 2011). Power generation for mining operations often occurs at mine site power plants, as is the case for Mount Keith. Thus, flue gases from these power plants could be circulated through tailings to directly offset mine emissions, as has been suggested for carbonation of other alkaline waste types such as cement kiln dust (Arickx et al., 2006). Although reaction rates would be lower, circulation of air rather than flue gas has the advantage that CO_2 leakage would not be a concern. Circulation of air is not an ideal solution because, due to the low CO_2 content in air, the carbonation rate would likely be limited by the rate of gas flow (i.e., CO_2 flux) that could be achieved. Thus, it could be advantageous to cap non-operational tailings storage facilities, such as TSF1, at active mines so that high concentrations of CO_2 could be used to ensure rapid carbonation of brucite while preventing leakage of CO_2 to the atmosphere.

Alternatively, water with elevated DIC concentrations, or at the least, water equilibrated with atmospheric CO_2 could be circulated through tailings. The effectiveness of injecting tailings with DIC-

charged water, air or flue gas is more likely to be limited by the flux of CO_2 that can be achieved in low permeability tailings (i.e., flow rate of water or gas; Fig. 11) than by the rate of brucite carbonation, which is rapid at elevated pCO_2. Assuming that the rate of CO_2 supply is the limiting factor, and that flow is governed by Darcy's law and driven by the natural elevation gradient at Mount Keith, it is estimated that the maximum CO_2 flux in the aqueous phase would be insufficient to carbonate all the brucite in TSF2 (Fig. 11, see Supporting Information for details on the calculations). Because even minor pressure gradients (e.g., <1 Pa/m) can strongly influence rates of gas advection (Thorstenson and Pollock, 1989) the assumption of elevation gradient driven flow was not applied for gas flow, but permeability constraints are expected to be less significant for the gas phase. In addition, in arid conditions, low water content allows high effective permeability for gas flow. These results imply that the use of CO_2-rich gas streams may therefore prove more effective than circulation of DIC-charged waters. In either case, however, the development of preferential flow paths and clogging of injection points will influence the efficiency of CO_2 delivery to all reactive phases.

Tailings permeability and clogging issues could be avoided by carbonating brucite within reactors in the ore processing plants at mine sites prior to deposition. For instance, flue gas from power generation could be supplied to reactors at ambient temperature and pressure. Given the observed abundance of brucite in ore and tailings, the mill at Mount Keith processes brucite at an average rate of 3.14×10^7 g brucite/h. Assuming a brucite carbonation rate of 7.78×10^{-3} g CO_2/g brucite/h with a 10% CO_2 gas stream (Harrison et al., 2013; for carbonation of a brucite slurry), the brucite in Mount Keith tailings could be carbonated at a rate commensurate to the rate at which it is processed at the mill. The disadvantage of this method is that the short reaction time required to carbonate the brucite would be insufficient to carbonate the less reactive phases such as serpentine minerals. In light of this, it may be preferable instead to continuously expose tailings to CO_2 through circulation of atmosphere or CO_2-rich water or gases to help drive carbonation of less reactive phases in addition to brucite, thereby increasing the overall mass of CO_2 that could be sequestered on the long term. Although the extent to

which CO_2 circulation would enhance Mg-silicate carbonation requires further investigation, Daval et al. (2013) reveal that elevated pCO_2 could accelerate lizardite dissolution by ~5-fold over pH-promoted dissolution alone at weakly acidic pH.

9. Geoengineering carbon neutral mines

The amount of tailings produced at Mount Keith in one year has the capacity to bind approximately 4 Mt of CO_2 (after Lackner et al., 1995 and estimates from Harrison et al., 2013). This exceeds the annual emissions of the mine by more than a factor of ten and represents more than a 100-fold increase of sequestration capacity over the current, passive rate of carbon mineralization (39 800 t/yr or approximately 11% of emissions). Importantly, the annual CO_2 sequestration capacity at Mount Keith is comparable to what is currently achieved at the largest demonstration projects for geologic CO_2 sequestration (approximately 1–2.8 Mt CO_2/yr; Michael et al., 2009; Whittaker et al., 2011; Harrison et al., 2013). Accelerating the rate of mineral carbonation within Mount Keith tailings to make use of 11% of its total capacity to capture and store atmospheric CO_2 would completely offset the greenhouse gas emissions produced by this mine. Further acceleration would provide a greenhouse gas benefit to the mine operator, which, if rigorously quantified, could be used to offset the cost of carbon credits in a cap-and-trade environment (Hitch and Dipple, 2012).

In the current regulatory climate in Australia, major emitters of greenhouse gases and producers of fossil fuels are liable to pay a carbon tax (i.e., $23 AUD per tonne of CO_2 in 2012–2013). Several major mining companies are subject to this tax under the carbon pricing mechanism. Enhancing the rate of carbon mineralization at Mount Keith to completely carbonate the brucite within tailings would offset between 20 and 60% of the mine's emissions (i.e., 20–60% of 370 kt/yr CO_2 equivalent emissions; Harrison et al., 2013). This offsetting represents a non-trivial financial benefit of $1.7M to $5.7M (AUD) per year, which translates to a lifetime value of $51M to $170M for a mine, such as Mount Keith, that has a 30-year operational lifetime. Our results indicate that such offsets may be

attained through a combination of changing tailings management practices and redesign of tailings compounds and ore processing circuits. Reinvention of tailings storage facilities as geoengineered landscapes and bioreactors may have further potential to enable ultramafic-hosted mines to leverage their full capacity to bind CO_2 within carbonate minerals (Power et al. 2009, 2010, 2011). For instance, Power et al. (2011) estimate that up to 16.7% of annual greenhouse gas emissions at Mount Keith could be offset by implementing coupled acid leaching and microbially mediated carbonate precipitation; this represents an increase over the current rate of passive emissions offsetting, which is approximately 11%. The tailings at Mount Keith alone provide the mine with the capacity not only to offset its own emissions but those of nine other comparably sized mining operations.

Globally, there is potential to sequester on the order of 400 Mt of CO_2/yr in the mineral waste from mines (Power et al., 2013). This represents an offsetting of approximately 1.5% of global annual greenhouse gas emissions (Power et al., 2013) or 16% of one carbon stabilization wedge (after Pacala and Socolow, 2004). Thus, by changing its tailings management practices to promote carbon mineralization, the international minerals industry has the capacity not only to achieve substantial offsetting of its own greenhouse gas emissions, but also to provide a tangible reduction to global CO_2 emissions.

Acknowledgements

We acknowledge the support of the Natural Sciences and Engineering Research Council of Canada (NSERC) and BHP Billiton through a Collaborative Research and Development Grant to GMD and GS. Funding was also provided by a grant from the Carbon Management Canada National Centre of Excellence to GMD and GS and through a Discovery Grant to MR. Work by SAW was supported by a Foundation Scholarship from the Mineralogical Association of Canada and an Alexander Graham Bell Canada Graduate Scholarship from NSERC. Work by IMP and ALH was supported by Post-Graduate Scholarships from NSERC. ALH was also supported by a University of British Columbia

Four-Year Fellowship. Thanks to Ben Grguric, Josh Levett, John Tomich, and all the staff at Mount Keith for their generous and knowledgeable support in the field. We would also like to thank Shelley Oliver, Claire Brown, Moira Cruickshanks, Vicky Liu, and Joanne Woodhouse for their skilled assistance in the laboratory, and Sergio Bea and Pejman Rasouli for sharing their modeling expertise. This study has benefited significantly from discussion with Alastair Sinclair and James Thom of the Department of Earth, Ocean and Atmospheric Sciences, UBC. This is publication xxx of the Mineral Deposit Research Unit.

References

Acero, P., Ayora, C., Carrera, J., Saaltink, M.W., Olivella, S., 2009. Multiphase flow and reactive transport model in vadose tailings. Applied Geochemistry 7, 1238–1250.

Acero, P., Ayora, C., Carrera, J., 2007. Coupled thermal, hydraulic and geochemical evolution of pyretic tailings in unsaturated column experiments. Geochimica et Cosmochimica Acta 71, 5325–5338.

Agnew, M., Taylor, G., 2000. Laterally extensive surface hardpans in tailings storage facilities as possible inhibitors of acid rock drainage. Proceedings of the 5th International Conference on Acid Rock Drainage, Society for Mining, Metallurgy, and Exploration, Inc., 1337–1346.

Arickx, S., van Gerven, T., Vandecasteele, C., 2006. Accelerated carbonation for treatment of MSWI bottom ash. Journal of Hazardous Materials B137, 235–243.

Assima, G.,P., Larachi, F., Beaudoin, G., Molson, J., 2013. Dynamics of carbon dioxide uptake in chrysotile mining residues – Effect of mineralogy and liquid saturation. International Journal of Greenhouse Gas Control 12, 124–135.

Australian Government Bureau of Meteorology, 2013. Climate Data Online: Daily Rainfall, Leinster Aeroport. http://www.bom.gov.au/climate/data/stations/.

Bachtiar, T., Coakley, J.P., Risk, M.J., 1996. Tracing sewage-contaminated sediments in Hamilton Harbour using selected geochemical indicators. Science of the Total Environment 179, 3–16.

Ballirano, P., De Vito, C., Ferrini, V., Mignardi, S., 2010. The thermal behaviour and structural stability of nesquehonite, $MgCO_3 \cdot 3H_2O$, evaluated by *in situ* laboratory parallel-beam X-ray powder diffraction: New constraints on CO_2 sequestration within minerals. Journal of Hazardous Materials 178, 522–528.

Barrett, F.M., Binns, R.A., Groves, D.I., Marston, F.J., McQueen, K.G., 1977. Structural history and metamorphic modification of Archean volcanic-type nickel deposits, Yilgarn Block, Western Australia. Economic Geology 77, 1195–1223.

Bea, S.A., Wilson, S.A., Mayer, K.U., Dipple, G.M., Power, I.M., Gamazo, P., 2012. Reactive transport modeling of natural carbon sequestration in ultramafic mine tailings. Vadose Zone Journal 11. doi: 10.2136/vzj2011.0053.

Beinlich, A., Austrheim, H., 2012. In situ sequestration of atmospheric CO_2 at low temperature and surface cracking of serpentinized peridotite in mine shafts. Chemical Geology 332–333, 32–44.

BHP Billiton, 2005. Mt Keith Nickel Operations: Environmental Data. BHP Billiton Sustainable Development Reports. http://hsecreport.bhpbilliton.com/wmc/2004/performance/mko/data/index.htm.

Bish, D.L., Howard, S.A., 1988. Quantitative phase analysis using the Rietveld method. Journal of Applied Crystallography 21, 86–91.

Blowes, D.W., Reardon, E.J., Jambor, J.L., Cherry, J.A., 1991. The formation and potential importance of cemented layers in inactive sulfide mine tailings. Geochimica et Cosmochimica Acta 55, 965–978.

Bobicki, E.R., Liu, Q., Xu, Z., Zeng, H., 2012. Carbon capture and storage using alkaline industrial wastes. Progress in Energy and Combustion Science 38, 302–320.

Bruker AXS, 2004a. EVA V. 10.0: Release 2004 – User's Manual: Karlsruhe, Germany, Bruker AXS.

Bruker AXS, 2004b. Topas V. 3.0: General Profile and Structure Analysis Software for Powder Diffraction Data. Bruker AXS, Germany.

Burnett, W.C., Schaeffer, O.A., 1980. Effect of ocean $^{13}C/^{12}C$ ratios in marine sediments from the New York Bight. Estuarine and Coastal Marine Sciences 11, 605–611.

Chacko, T., Cole, D.R., Horita, J., 2001. Equilibrium oxygen, hydrogen and carbon isotope fractionation factors applicable to geologic systems. In: Valley, J.W., Cole, D.R., (Eds.), Stable Isotope Geochemistry. Reviews in Mineralogy and Geochemistry 43, 1–81.

Cheary, R.W., Coelho, A.A., 1992. A fundamental parameters approach to X-ray line-profile fitting. Journal of Applied Crystallography 25, 109–121.

Chipera, S., Vaniman, D.T., 2007. Experimental stability of magnesium sulfate hydrates that may be present on Mars. Geochimica et Cosmochimica Acta 71, 241–250.

Chou, I.M., Seal, R.R., II, 2007. Magnesium and calcium sulfate stabilites and the water budget of Mars. Journal of Geophysical Research 112, E11004, doi: 10.1029/2007JE002898.

Chou, I.M., Seal, R.R., II, 2003. Determination of epsomite-hexahydrite equilibria by the humidity-buffer technique at 0.1 MPa with implications for phase equilibria in the system $MgSO_4$-H_2O. Astrobiology 3, 619–630.

Daval, D., Hellmann, R., Martinez, I., Gangloff, S., Guyot, F., 2013. Lizardite serpentine dissolution kinetics as a function of pH and temperature, including effects of elevated pCO_2. Chemical Geology, in press, doi: 10.1016/j.chemgeo.2013.05.020.

deBruyn, A.M.H., Rasmussen, J.B., 2002. Quantifying assimilation of sewage-derived organic matter by riverine benthos. Ecological Applications 12, 511–520.

de Choudens-Sánchez, V., González, L.A., 2009. Calcite and aragonite precipitation under controlled instantaneous supersaturation: Elucidating the role of $CaCO_3$ saturation state and Mg/Ca ratio on calcium carbonate polymorphism. Journal of Sedimentary Research 6, 363–376.

Power, I.M., Harrison, A.L., Dipple, G.M., Wilson, S.A., Kelemen, P.B., Hitch, M., Southam, G., 2013. Ex situ carbon mineralization: From natural analogues to engineered systems. Reviews in Mineralogy and Geochemistry, in review.

Dold, B., 2006. Element flows associated with marine shore mine tailings deposits. Environmental Science & Technology 40, 752–758.

Donahue, D.J., Linick, T.W., Jull, A.J.T., 1990. Isotope-ratio and background corrections for accelerator mass spectrometry radiocarbon measurements. Radiocarbon 32, 135–142.

Fernandes, S.A.P., Bettiol, W., Cerri, C.C., Camargo, P., 2005. Sewage sludge effects on gas fluxes at the soil-atmosphere interface, on soil $\delta^{13}C$ and on total soil carbon and nitrogen. Geoderma 125, 49–57.

Ferrini, V., De Vito, C., Mignardi, S., 2009. Synthesis of nesquehonite by reaction of gaseous CO_2 with Mg chloride solution: Its potential role in the sequestration of carbon dioxide. Journal of Hazardous Materials 168, 832–837.

Gearing, P.J., Gearing, J.N., Maughan, J.T., Ovlatt, C.A., 1991. Isotopic distribution of carbon from sewage sludge and eutrophication in the sediments and food web of estuarine ecosystems. Environmental Science & Technology 25, 295–301.

Grguric, B.A., 2003. Minerals of the MKD5 nickel deposit, Mount Keith, Western Australia. Australian Journal of Mineralogy 9, 55–71.

Grguric, B.A., Madsen, I.C., Pring, A., 2001. Woodallite, a new chromium analogue of iowaite from the Mount Keith nickel deposit, Western Australia. Mineralogical Magazine 65, 427–435.

Grguric, B.A., Rosengren, N.M., Fletcher, C.M., Hronsky, J.M.A., 2006. Type 2 deposits: geology, mineralogy and processing of the Mount Keith and Yakabindi orebodies, Western Australia. Society of Economic Geologists Special Publications 13, 119–138.

Hänchen, M., Prigiobbe, V., Baciocchi, R., Mazzotti, M., 2008. Precipitation in the Mg-carbonate system–effects of temperature and CO_2 pressure 63, 1012–1028.

Hansen, L.D., 2005. Geologic setting of listwanite, Atlin, B.C.: Implications for carbon dioxide sequestration and lode-gold mineralization. Unpublished M.Sc. thesis. The University of British Columbia, Vancouver, Canada. 174 pp.

Harrison, A.L., Power, I.M., Dipple, G.M., 2013. Accelerated carbonation of brucite in mine tailings for carbon sequestration. Environmental Science & Technology 47, 126–134.

Hill, R.E.T., Barnes, S.J., Gole, M.J., Dowling, S.E., 1990. The physical volcanology of komatiites in the Norseman-Wiluna belt. In: Ho, S.E., Glover, J.E., Myers, J.S., Muhling, J.R. (Eds.), Third International Archean Symposium, Perth 1990, Excursion Guidebook. University of Western Australia, 362–397.

Hill, R.J., Howard, C.J., 1987. Quantitative phase analysis from neutron powder diffraction data using the Rietveld method. Journal of Applied Crystallography 20, 467–474.

Hitch, M., Dipple, G.M., 2012. Economic feasibility and sensitivity analysis of integrating industrial-scale mineral carbonation into mining operations. Minerals Engineering 39, 268–275.

Hostetler, P.B., Coleman, R.G., Mumpton, F.A., Evans, B.W., 1966. Brucite in alpine serpentinites. American Mineralogist 51, 75–98.

Hövelmann, J., Putnis, C.V., Ruiz-Agudo, E., Austrheim, H., 2012. Direct nanoscale observations of CO_2 sequestration during brucite [$Mg(OH)_2$] dissolution. Environmental Science & Technology 46, 5253–5260.

Huijgen, W.J.J., Comans, R.N.J., 2005. Carbon dioxide sequestration by mineral carbonation: Literature review update 2003-2004. Energy Research Centre of the Netherlands, Report ECN-C-05-022.

Huijgen, W.J.J., Comans, R.N.J., 2003. Carbon dioxide sequestration by mineral carbonation: Literature review. Energy Research Centre of the Netherlands, Report ECN-C-03-016.

Huntzinger, D.N., Gierke, J.S., Kawatra, S.K., Eisele, T.C., Sutter, L.L., 2009. Carbon dioxide sequestration in cement kiln dust through mineral carbonation. Environmental Science & Technology 43, 1986–1992.

IAEA/WMO, 2012. International Atomic Energy Agency and World Meteorological Organization Global Network of Isotopes in Precipitation Database. [http://www-naweb.iaea.org/napc/ih/IHS_resources_gnip.html]

IPCC, 2005. IPCC Special Report on Carbon Dioxide Capture and Storage. Metz, B., Davidson, O., de Coninck, H.C., Loos, M., and Meyer, L.A. (Eds.). Cambridge University Press, Cambridge, UK and New York, NY, U.S.A. 431 pp.

Jambor, J.L., Nordstrom, D.K., Alpers, C.N., 2000. Metal-sulfate salts from sulfide mineral oxidation. In: Alpers, C.N., Jambor, J.L., Nordstrom, D.K. (Eds.), Sulfate Minerals: Crystallography,

Geochemistry, and Environmental Significance. Reviews in Mineralogy and Geochemistry 40, 303–350.

Jambor, J.L., Blowes, D.W., 1998. Theory and applications of mineralogy in environmental studies of sulfide-bearing mine wastes. In: Cabri, L.J., Vaughn, D.J. (Eds.), Modern Approaches to Ore and Environmental Mineralogy. Mineralogical Association of Canada Short Course 27, 367–401.

Jeen, S.-W., Gillham, R.W., Blowes, D.W., 2006. Effects of carbonate precipitates on long-term performance of granular iron for reductive dechlorination of TCE. Environmental Science & Technology 40, 6432–6437.

Kenward, P.A., Goldstein, R.H., González, L.A., Roberts, J.A., 2009. Precipitation of low temperature dolomite from an anaerobic microbial consortium: The role of methanogenic Archaea. Geobiology 7, 556–565.

Kikkinedes, E.S., Yang, R.T., Cho, S.H., 1993. Concentration and recovery of CO_2 from flue gas by pressure swing adsorption. Industrial & Engineering Chemistry Research 32, 2714–2720.

Königsberger, E., Königsberger, L., Gamsjager, H., 1999. Low-temperature thermodynamic model for the system Na_2CO_3-$MgCO_3$-$CaCO_3$-H_2O. Geochimica et Cosmochimica Acta 63, 3105–3119.

Kralik, M., Aharon, P., Schroll, E., Zachmann, D., 1989. Carbon and oxygen isotope systematics of magnesites: A review. In: Möller, P. (Ed.), Magnesite: Geology, Mineralogy, Geochemistry, Formation of Mg-Carbonates. Monograph Series on Mineral Deposits 28, 197–223.

Lackner, K.S., 2003. Climate change: A guide to CO_2 sequestration. Science 300, 1677–1678.

Lackner, K.S., Wendt, C.H., Butt, D.P., Joyce, G.L., Sharp, D.H., 1995. Carbon dioxide disposal in carbonate minerals. Energy 20, 1153–1170.

Levin, I., Hammer, S., Kromer, B., Meinhardt, F., 2008. Radiocarbon observations in atmospheric CO_2: Determining fossil fuel CO_2 over Europe using Jungfraujoch observations as background. Science of the Total Environment 391, 211–216.

Manning, D.A.C., Renforth, P., 2013. Passive sequestration of atmospheric CO_2 through coupled plant–mineral reactions in urban soils. Environmental Science & Technology 47, 135–141.

Manning, D.A.C., 2008. Biological enhancement of soil carbonate precipitation: passive removal of atmospheric CO_2. Mineralogical Magazine 72, 639–649.

Mayer, K.U., Frind, E.O., Blowes, D. W., 2002. Multicomponent reactive transport modeling in variably saturated porous media using a generalized formulation for kinetically controlled reactions. Water Resources Research 38, 1174.

Michael, K., Allinson, G., Golab., A., Sharma, S., Shulakova, V., 2009. CO_2 storage in saline squifers II – experience from existing storage operations. Energy Procedia 1, 1973–1980.

Mills, S.J., Wilson, S.A., Dipple, G.M., Raudsepp, M., 2010. The decomposition of konyaite: importance in CO_2 fixation in mine tailings. Mineralogical Magazine 75, 903–917.

Nicholson, R.V., Gillham, R.W., Reardon, E.J., 1989. Pyrite oxidation in carbonate-buffered solution: 2. Rate control by oxide coatings. Geochimica et Cosmochimica Acta 54, 395–402.

O'Neil, J.R., Barnes, I., 1971. C^{13} and O^{18} compositions in some fresh-water carbonates associated with ultramafic rocks and serpentinites: Western United States. Geochimica et Cosmochimica Acta 35, 687–697.

Pacala, S, Socolow, R., 2004. Stabilization wedges: solving the climate problem for the next 50 years with current technologies. Science 305, 968–972.

Palandri, J.L., Kharaka, Y.K., 2004. A compilation of rate parameters of water-mineral interaction kinetics for application to geochemical modelling. U.S. Geological Survey Open File Report 2004-1068.

Pokrovsky, O.S., Schott, J., 2004. Experimental study of brucite dissolution and precipitation in aqueous solutions: Surface speciation and chemical affinity control. Geochimica et Cosmochimica Acta 68, 31–45.

Power, I.M., Wilson, S.A., Dipple, G.M., 2013. Serpentinite carbonation for CO_2 sequestration. Elements 9, 115–121.

Power, I.M., Wilson, S.A., Small, D.P., Dipple, G.M., Wan, W.K., Southam, G., 2011. Microbially mediated mineral carbonation: Roles of phototrophy and heterotrophy. Environmental Science & Technology 45, 9061–9068.

Power, I.M., Dipple, G.M., Southam, G., 2010. Bioleaching of ultramafic tailings by *Acidithiobacillus* spp. for CO_2 sequestration. Environmental Science & Technology 44, 456–462.

Power, I.M., Wilson, S.A., Thom, J.M., Dipple, G.M., Gabites, J.E., Southam, G., 2009. The hydromagnesite playas of Atlin, British Columbia, Canada: A biogeochemical model for CO_2 sequestration. Chemical Geology 260, 286–300.

Power, I.M., Wilson, S.A., Thom, J., Dipple, G.M., Southam, G., 2007. Biologically induced mineralization of dypingite by cyanobacteria from an alkaline wetland near Atlin, British Columbia, Canada. Geochemical Transaction 8, article 13.

Pronost, J., Beaudoin, G., Lemieux, J.-M., Hébert, R., Constantin, M., Marcouiller, S., Klein, M., Duchesne, J., Molson, J.W., Larachi, F., Maldague, X., 2012. CO_2-depleted warm air venting from chrysotile milling waste (Thetford Mines, Canada): Evidence for in-situ carbon capture from the atmosphere. Geology 40, 275–278.

Pronost, J., Beaudoin, G., Tremblay, J., Larachi, F., Duchesne, J., Hébert, R., Constantin, M., 2011. Carbon sequestration kinetic and storage capacity of ultramafic mining waste. Environmental Science & Technology 45, 9413–9420.

Ramírez-Álvarez, N., Macías-Zamora, J.V., Burke, R.A., Rodríguez-Villanueva, L.V., 2007. Use of $\delta^{13}C$, $\delta^{15}N$, and carbon to nitrogen ratios to evaluate the impact of sewage-derived particulate organic matter on the benthic communities of the Southern California Bight. Environmental Toxicology and Chemistry 26, 2332–2338.

Raudsepp, M., Pani, E., 2003. Application of Rietveld analysis to environmental mineralogy. In: Jambor, J.L., Blowes, D.W., Ritchie, A.I.M. (Eds.), Environmental Mineralogy of Mine Wastes. Mineralogical Association of Canada Short Course 31, 165–180.

Reimer, P.J., Brown, T.A., Reimer, R.W., 2004. Discussion: Reporting and calibration of post-bomb ^{14}C data. Radiocarbon 46, 1299–1304.

Renaut, R.W., Stead, D., 1991. Recent magnesite-hydromagnesite sedimentation in the playa basins of the Cariboo Plateau, British Columbia. Geological Fieldwork (BCGSB), Paper 1991-1, 279–288.

Renaut, R.W., 1990. Recent carbonate sedimentation and brine evolution in the saline lake basins of the Cariboo Plateau, British Columbia, Canada. Hydrobiologia 197, 67–81.

Renaut, R.W., Long, P.R., 1989. Sedimentology of the saline lakes of the Cariboo Plateau, Interior British Columbia, Canada. Sedimentary Geology 64, 239–264.

Renforth, P., Washbourne, C.-L., Taylder, J., Manning, D.A.C., 2011. Silicate production and availability for mineral carbonation. Environmental Science & Technology 45, 2035–2041.

Renforth, P., Manning, D.A.C., Lopez-Capel, E., 2009. Carbonate precipitation in artificial soil as a sink for atmospheric carbon dioxide. Applied Geochemistry 24, 1757–1764.

Rietveld, H.M., 1969. A profile refinement method for nuclear and magnetic structures. Journal of Applied Crystallography 2, 65–71.

Roselle, G.T., Baumgartner, L.P., Valley, J.W., 1999. Stable isotope evidence of heterogeneous fluid infilration at the Ubehebe Peak contact aureole, Death Valley National Park, California. American Journal of Science 299, 93–138.

Seifritz, W., 1990. CO_2 disposal by means of silicates. Nature 345, 486.

Sipilä, J., Teir, S., Zevenhoven, R., 2008. Carbon dioxide sequestration by mineral carbonation: Literature review update 2005-2007. Åbo Akademi University Heat Engineering Laboratory, Report 2008-1.

Spies, R.B., Kruger, H., Ireland, R., Rice, D.W., Jr., 1989. Stable isotope ratios and contaminant concentrations in a sewage-distorted food web. Marine Ecology Progress Series 54, 157–170.

Stolberg, D.J., 2005. Rehabilitation studies on tailings storage facilities in an arid hypersaline region. Unpublished Ph.D. thesis. The University of Queensland, Brisbane, Australia. 304 pp.

Tasse, N., Germain, D, Dufour, C., Tremblay, R., 1997. Hardpan formation in the Canadian Malartic Mine tailings: Implications for the reclamation of the abandoned impoundments. Proceedings of the 4th International Conference on Acid Rock Drainage, MEND, Natural Resources Canada, 1797–1812.

Thom, J.G.M., Dipple, G.M., Power, I.M., Harrison, A.L., (2013). Chrysotile dissolution rates: Implications for carbon sequestration. Applied Geochemistry, in press. doi: 10.1016/j.apgeochem.2013.04.016.

Thorstenson, D.C., Pollock, D.W., 1989. Gas transport in unsaturated porous media: The adequacy of Fick's law. Reviews of Geophysics 27, 61–78.

Uibu, M., Kuusik, R., Andreas, L., Kirsimaë, K., 2011. The CO_2-binding by Ca-Mg-silicates in direct aqueous carbonation of oil shale ash and steel slag. Energy Procedia 4, 925–932.

Upton, G., Cook, I., 2008. A Dictionary of Statistics. Oxford University Press, U.S.A. 512 pp.

Van Dover, C.L., Grassle, J.F., Fry, B., Garritt, R.H., Starczak, V.R., 1992. Stable isotope evidence for entry of sewage-derived organic material into a deep-sea food web. Nature 360, 153–156.

Warren, J.K., 2006. Evaporites: Sediments, Resources, and Hydrocarbons. Springer-Verlag, Germany. 1035 pp.

Whittaker, S., Rostron, B., Hawkes, C., Gardner, C., White, D., Johnson, J., 2011. A decade of CO_2 injection into depleting oil fields: monitoring and research activities of the IEA GHG Weyburn-Midale CO_2 Monitoring and Storage Project. Energy Procedia 4, 6069–6076.

Wilson, S.A., Dipple, G.M., Power, I.M., Barker, S.L.L., Fallon, S.J., Southam, G., 2011. Subarctic weathering of mineral wastes provides a sink for atmospheric CO_2. Environmental Science & Technology 45, 7727–7736.

Wilson, S.A., Barker, S.L.L., Dipple, G.M., Atudorei, V., 2010, Isotopic disequilibrium during uptake of atmospheric CO_2 into mine process waters: Implications for CO_2 sequestration. Environmental Science & Technology 44, 9522–9529.

Wilson, S.A., 2009. Mineral traps for greenhouse gases in mine tailings: A protocol for verifying and quantifying CO_2 sequestration in ultramafic mines. Unpublished Ph.D. thesis. The University of British Columbia, Vancouver, Canada. 315 pp.

Wilson, S.A., Dipple, G.M., Power, I.M., Thom, J.M., Anderson, R.G., Raudsepp, M., Gabites, J.E., Southam, G., 2009a. Carbon dioxide fixation within mine wastes of ultramafic-hosted ore deposits: Examples from the Clinton Creek and Cassiar chrysotile deposits, Canada. Economic Geology 104, 95–112.

Wilson, S.A., Raudsepp, M., Dipple, G.M., 2009b. Quantifying carbon fixation in trace minerals from processed kimberlite: A comparative study of quantitative methods using X-ray powder diffraction data with applications to the Diavik Diamond Mine, Northwest Territories, Canada. Applied Geochemistry 24, 2312–2331.

Wilson, S.A., Raudsepp, M., Dipple, G.M., 2006. Verifying and quantifying carbon fixation in minerals from serpentine-rich mine tailings using the Rietveld method with X-ray powder diffraction data. American Mineralogist 91, 1331–1341.

Xiong, Y., Lord, A.S., 2008. Experimental investigations of the reaction path in the $MgO\text{-}CO_2\text{-}H_2O$ system in solutions with various ionic strengths, and their applications to nuclear waste isolation. Applied Geochemistry 23, 1634–1659.

Yanful, E.K., St-Arnaud, L.C., 1992. Migration of acidic pore waters at the Waite Amulet tailings site near Rouyn-Noranda, Quebec, Canada. Canadian Geotechnical Journal 29, 466–476.

Zevenhoven, R., Fagerlund, J., Songok, J.K. 2011. CO_2 mineral sequestration: Developments toward large-scale application. Greenhouse Gases: Science and Technology 1, 48–57.

Zhang, P., Anderson, H.L.J., Kelly, J.W., Krumhansl, J.L., Papenguth, H.W., 2000. Kinetics and mechanisms of formation of magnesite from hydromagnesite in brine. Sandia National Laboratories, Albuquerque, p 26.

Zhao, L., Sang., L, Chen, J., Ji, J., Teng, H.H., 2010. Aqueous carbonation of natural brucite: Relevance to CO_2 sequestration. Environmental Science & Technology 44, 406–411.

Figure Captions

Fig. 1. a) The Tailings Storage Facilities (TSFs) at Mount Keith. b) Location of Mount Keith Nickel Mine within Australia.. The roughly circular facility in (a) is TSF2 and the smaller, adjoining facility is TSF1. Samples were collected at 59 locations in TSF1 and TSF2. Sampling in TSF2 was done along the perimeter of the facility and on both sides of a radial access road. Sampling in TSF1 was done proximal to the access road in Cell 2 (the right-most cell of TSF1). Squares indicate sites sampled in 2005; circles indicate sites sampled in 2006; borders on circles indicate sites for which Rietveld refinements have been done; Triangles indicate locations of risers from which tailings are deposited. Shading denotes regions of the TSFs in which deposition of tailings had ceased as of 2006.

Fig. 2. Backscattered electron images of hydromagnesite in Mount Keith mine tailings. Both a) and b) are from a particularly hydromagnesite-rich sample, 06MK9-9. a) Hydromagnesite crystals precipitating at the surface of larger grains of serpentine and infilling cracks and fissures within them. b) Hydromagnesite cementing both fine and larger grains of serpentine and magnetite together. H – hydromagnesite; M – magnetite; S – serpentine.

Fig. 3. Mount Keith mine tailings at the surface and at depth within TSF2. a) The upper half of the profile at sampling site 1 (06MKP1). Numbers label specific samples (e.g., "1" denotes sample "06MKP1-1") and white lines separate distinct horizons. b) The profile excavation from a) and a 5m x 5m grid sample (delineated by the blue tarpaulin) at sampling site 1. c) Backhoe excavation at sampling site 30, showing near surface water and meter-scale desiccation cracks. d) An older surface in TSF2 (~1-year old) showing well-developed efflorescences and more pervasive desiccation features. e) The 7–8-year old surface of TSF2 at sampling site 9 (showing sample 06MK9-6), which is heavily cemented with hydromagnesite.

Fig. 4. Variation of hydromagnesite abundance with depth beneath the surface of TSF2 over time. Age is measured relative to 2006, the date of sampling. Open circles indicate the median depth from which a sample was taken. The associated vertical lines represent intervals of depth over which individual samples were collected. Lines drawn through the data for tailings of each age connect points that denote the mean depth of sampling (based on median depths for individual samples) and the median abundance of hydromagnesite for samples from similar depths. Shaded regions are the median value ± the median absolute deviation. Black and red lines represent model output from modelling of the hydromagnesite burial and process water replenishment hypotheses, respectively.

Fig. 5. Variation of the abundance of select secondary minerals (hydromagnesite, halite, blödite and gypsum) with depth beneath the surface of TSF2 over time. Age is measured relative to 2006, the date of sampling.

Fig. 6. Variation of the abundance of gangue carbonate minerals (hydrotalcite-group, calcite, dolomite and magnesite) compared to hydromagnesite abundance with depth beneath the surface of TSF2 over time. Age is measured relative to 2006, the date of sampling.

Fig. 7. Variation of the abundance of brucite and serpentine-group minerals compared to hydromagnesite abundance with depth beneath the surface of TSF2 over time. Age is measured relative to 2006, the date of sampling.

Fig. 8. Stable oxygen and carbon isotope data for different modes of occurrence and mineralogy of carbonate minerals at Mount Keith. Numbers label fields for Mg-carbonate minerals in equilibrium with specific reservoirs for carbon. Measurement errors (as 2σ) are typically smaller than the symbols employed.

Fig. 9. Stable carbon ($\delta^{13}C$) and fraction modern carbon ($F^{14}C$) data for secondary precipitates of hydromagnesite, bedrock carbonate minerals, and soda ash (a process additive) from Mount Keith. Numbers label fields for Mg-carbonate minerals in equilibrium with specific reservoirs for carbon. Values for $\delta^{13}C$ were determined in the Pacific Centre for Isotopic and Geochemical Research at the University of British Columbia. Values for $F^{14}C$ are corrected for machine fractionation using AMS results for $\delta^{13}C$. Measurement errors are typically smaller than the symbols employed.

Fig. 10. Amount of brucite remaining in a 2 cm thick band of tailings versus time at different rates of tailings deposition (brucite burial rate) as estimated using model output.

Fig. 11. Brucite carbonation rate versus saturated hydraulic conductivity. Solid lines represent potential carbonation rates achieved with water equilibrated with atmospheric CO_2 (~0.04% CO_2), 10% CO_2, and 100% CO_2 gas at 1 atm pressure and 25°C. All calculations are for a 50 cm thick tailings deposit representative of 1 year's worth of tailings deposition at the Mount Keith mine. The horizontal dashed line indicates the minimum carbonation rate that would be necessary to carbonate all the brucite (i.e., 2.5 wt.%) in 50 cm of tailings within 1 year. Refer to the Supporting Information for details regarding the calculations.

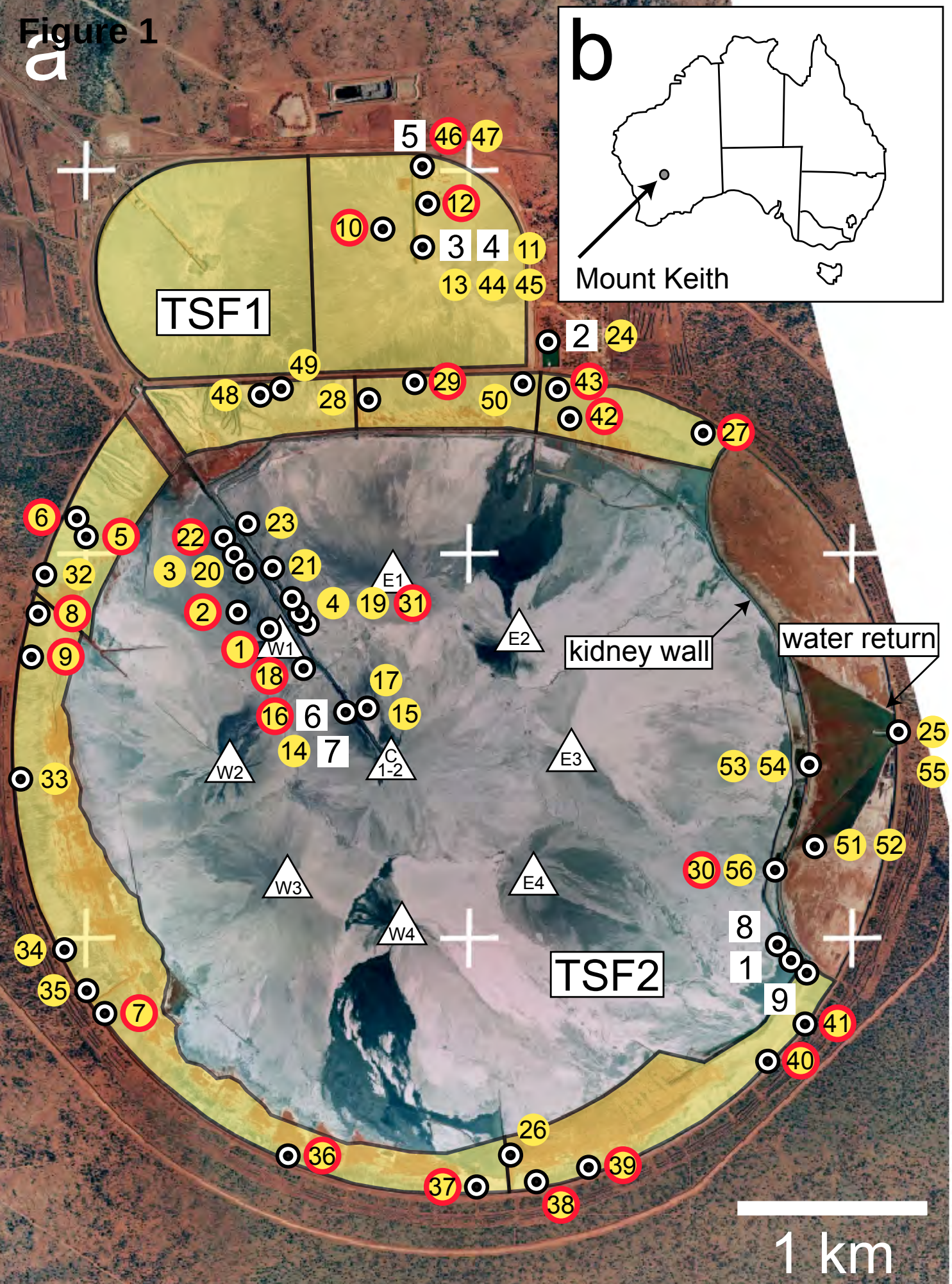
Figure 1
a
b
Mount Keith
TSF1
TSF2
kidney wall
water return
E1
E2
E3
E4
W1
W2
W3
W4
C 1-2
1 km

Figure 2

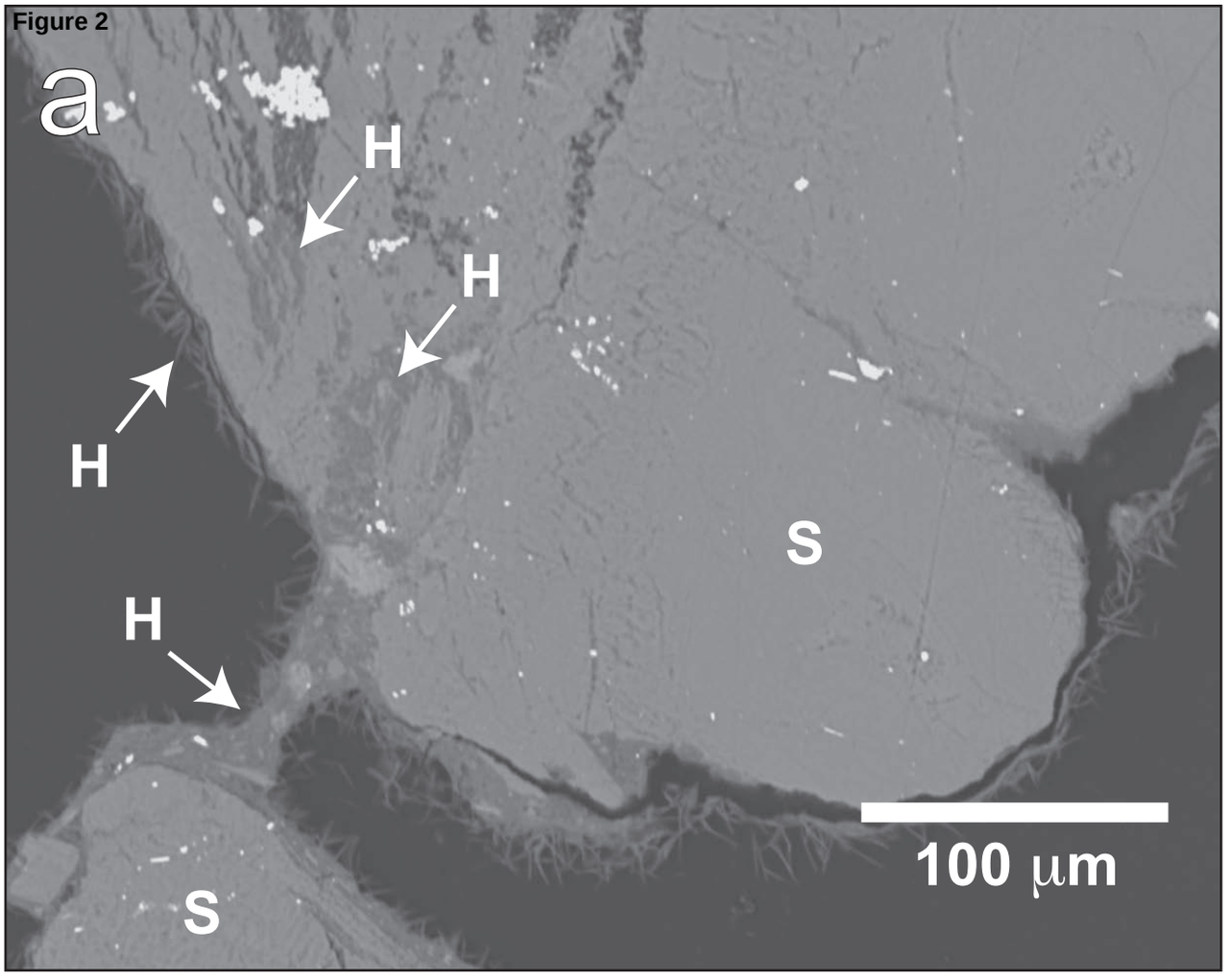

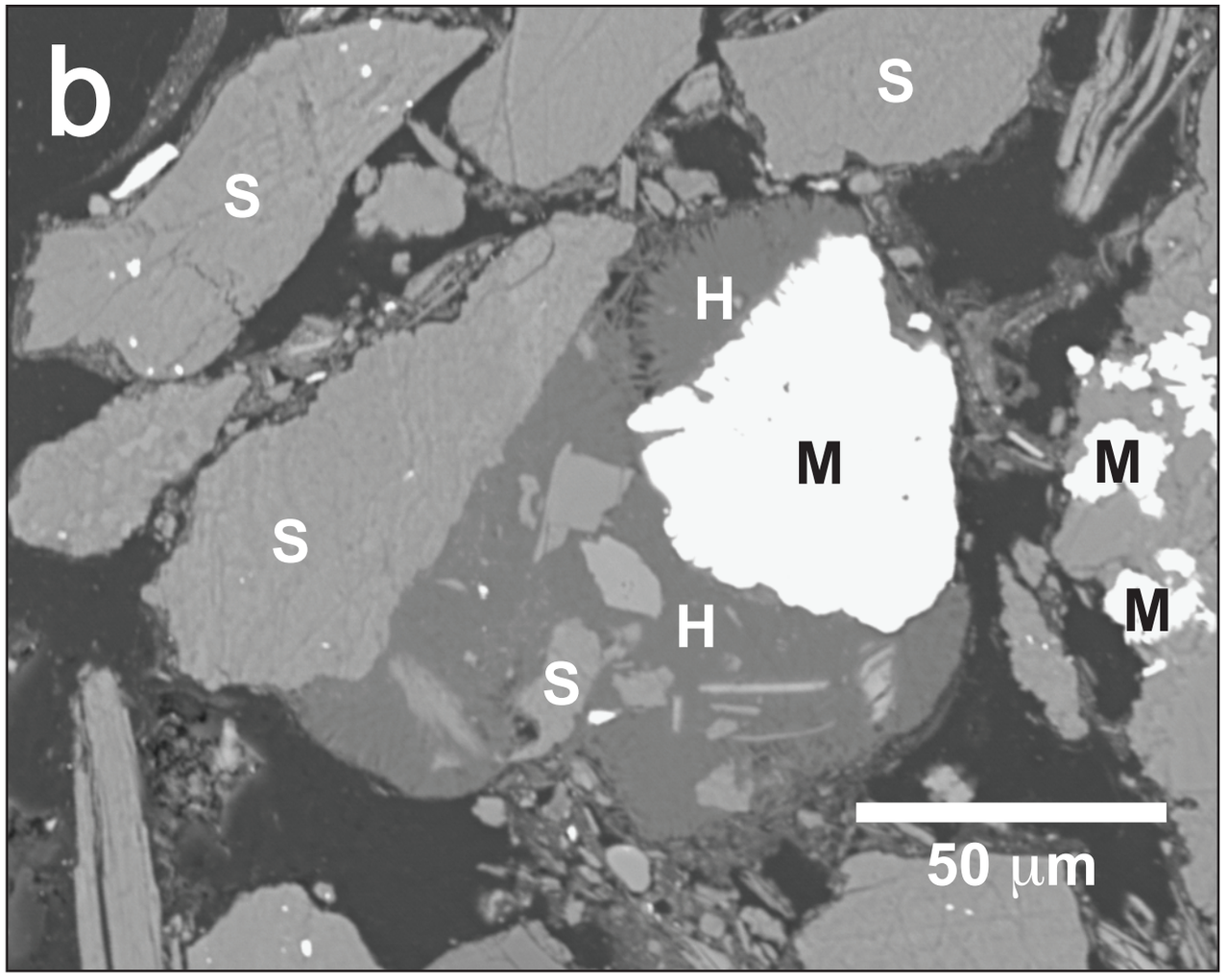

Figure 3

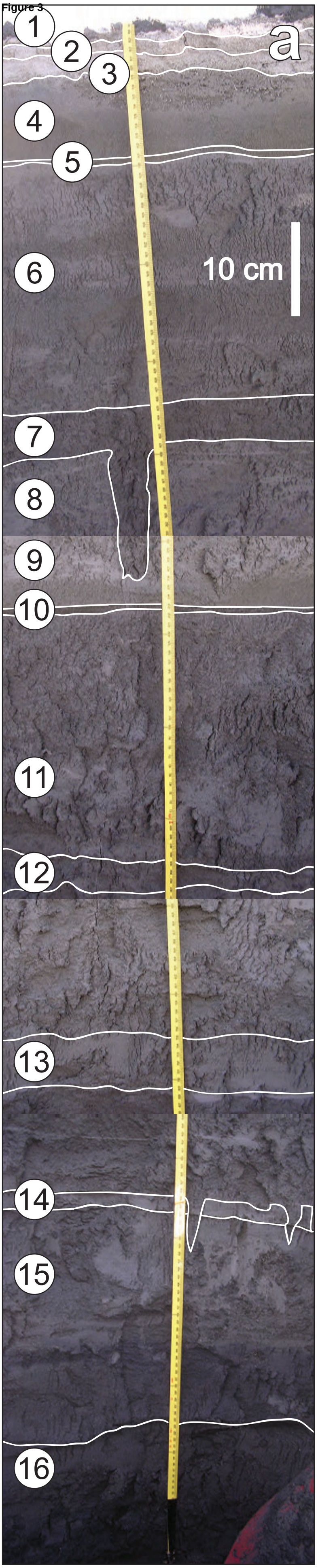

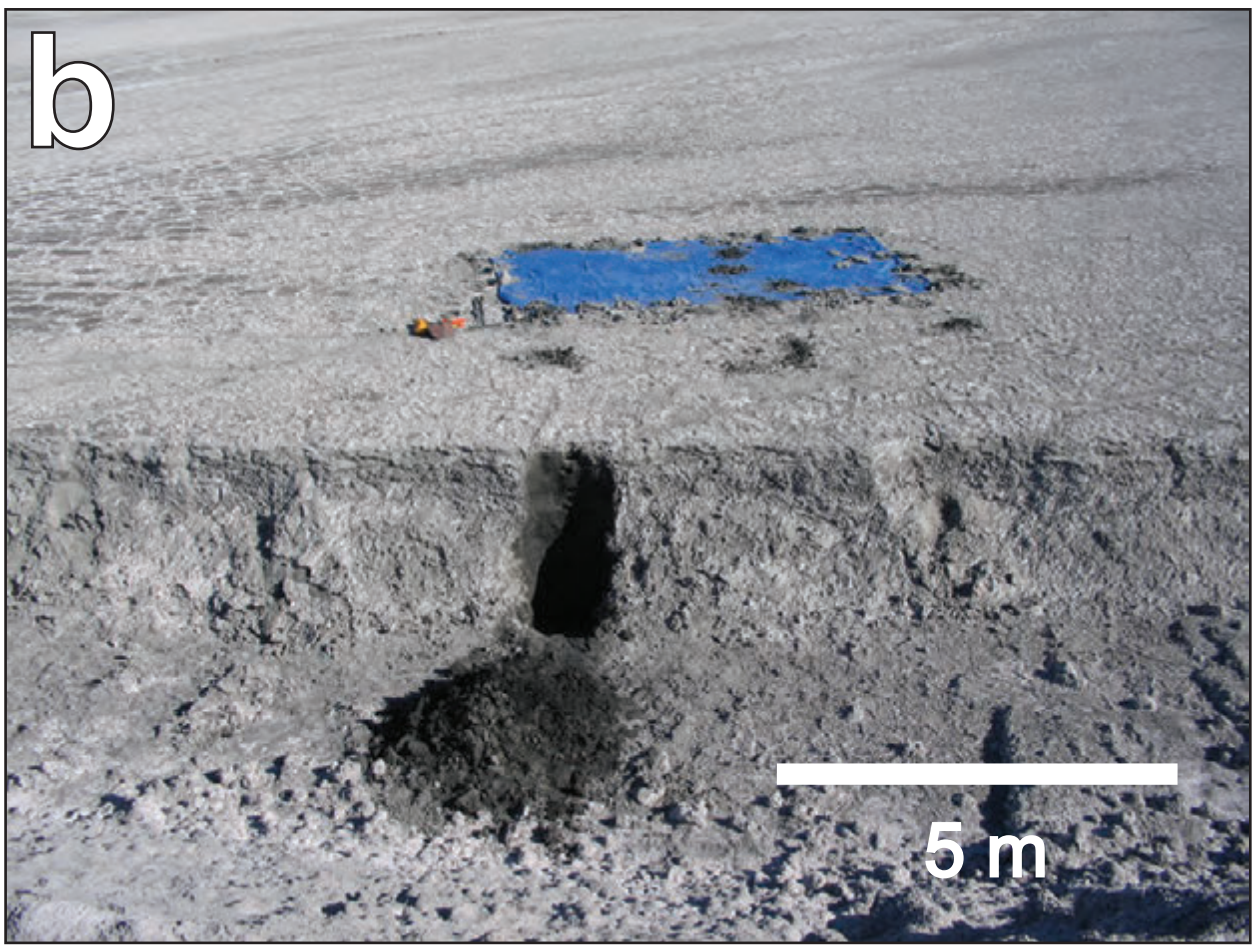

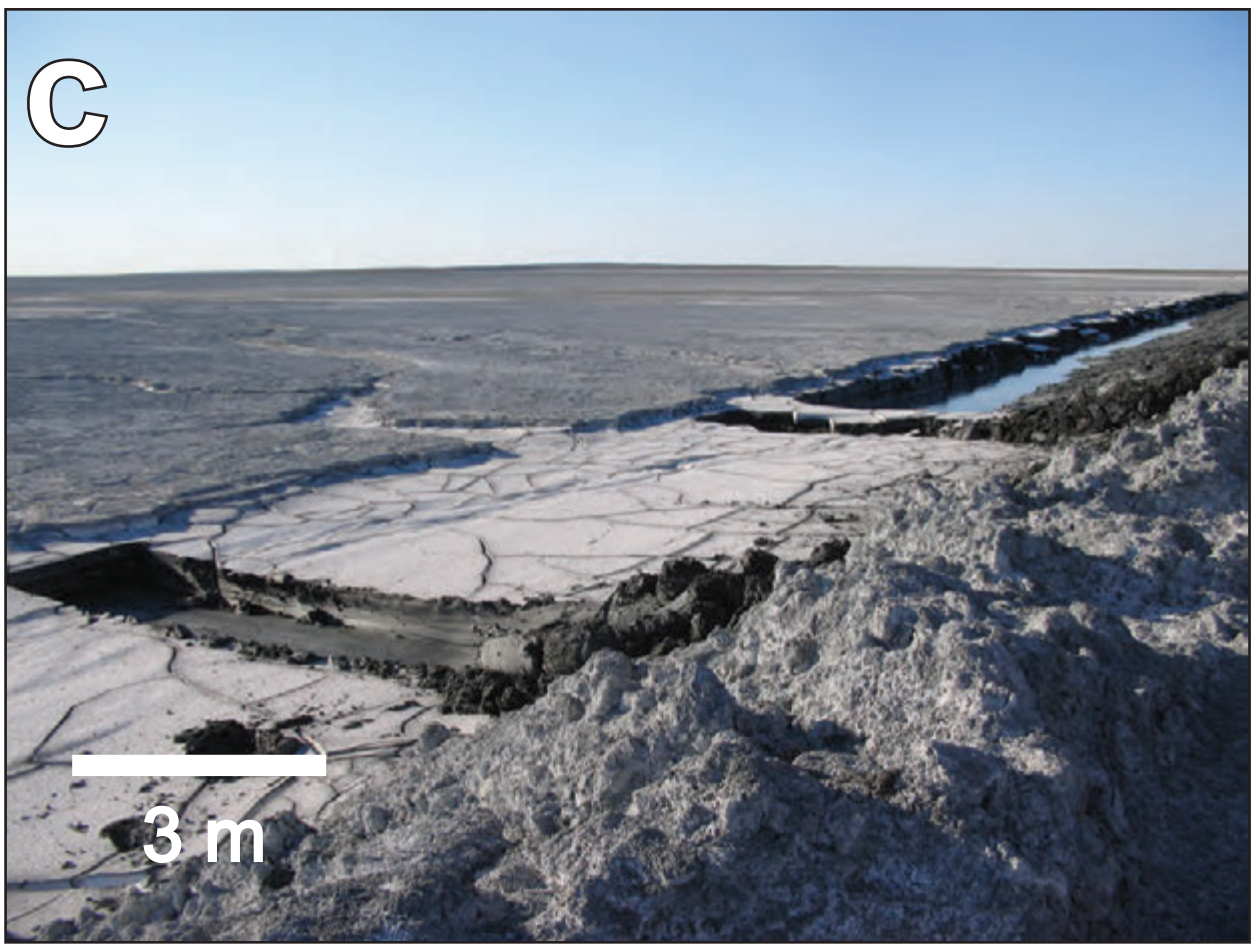

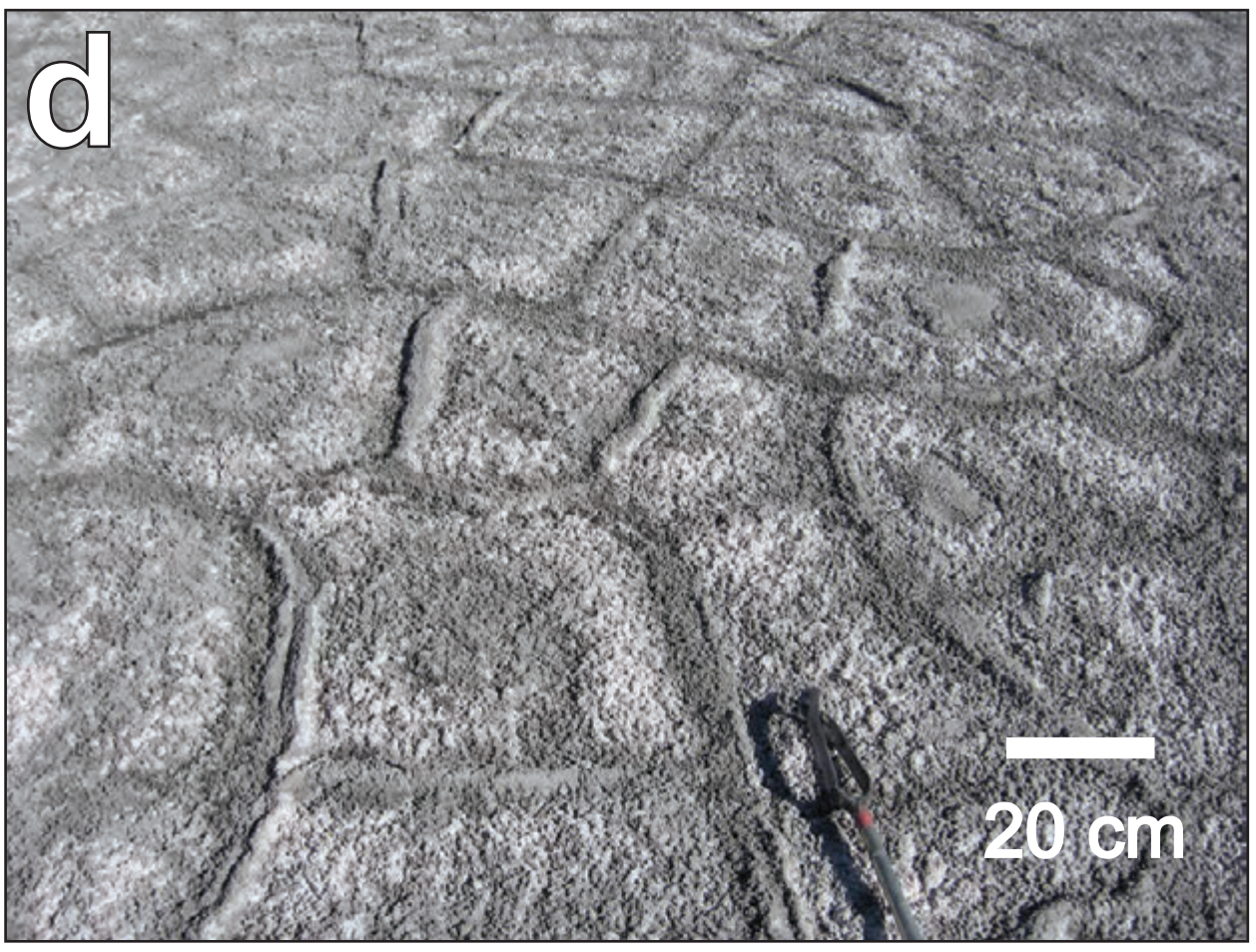

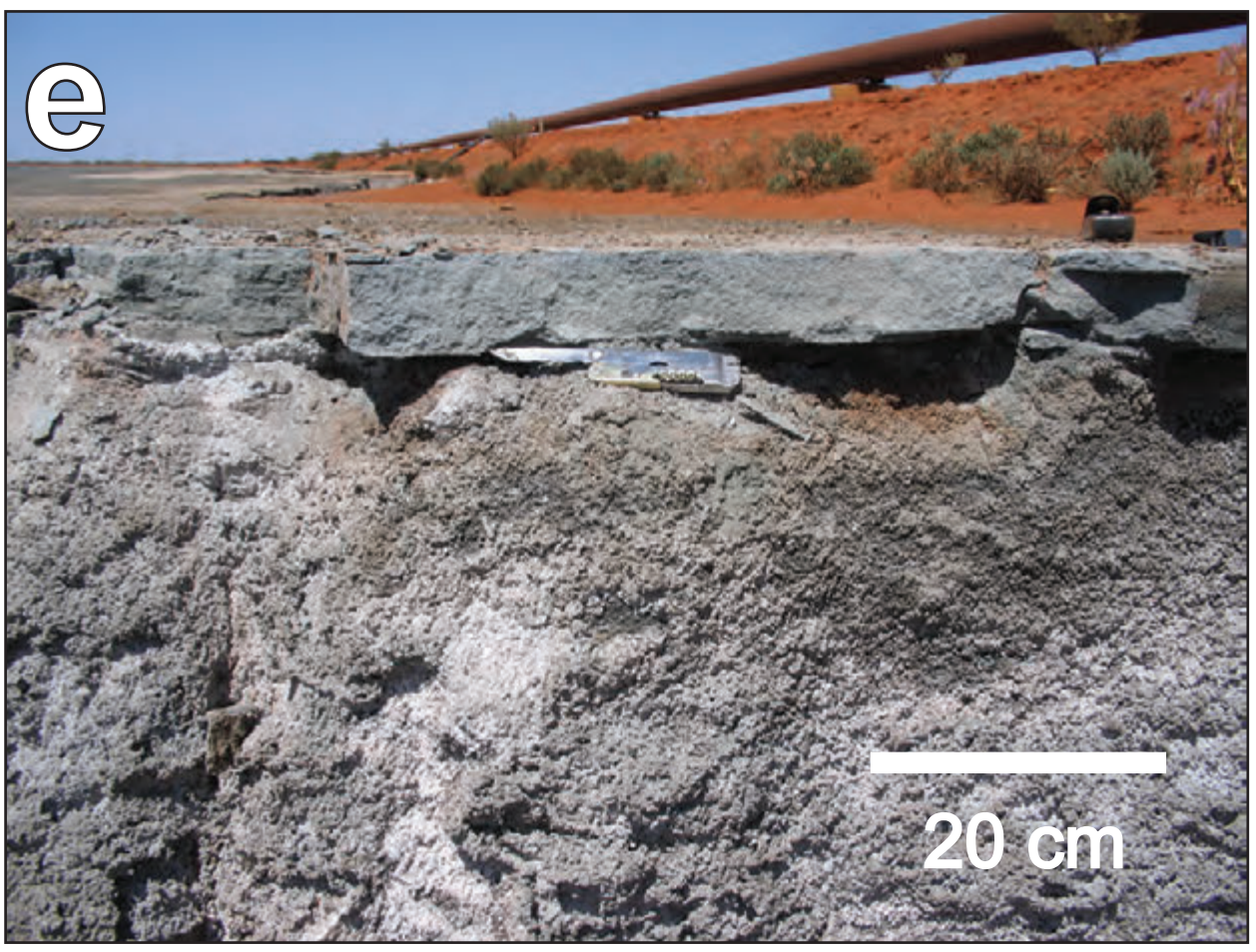

Figure 4

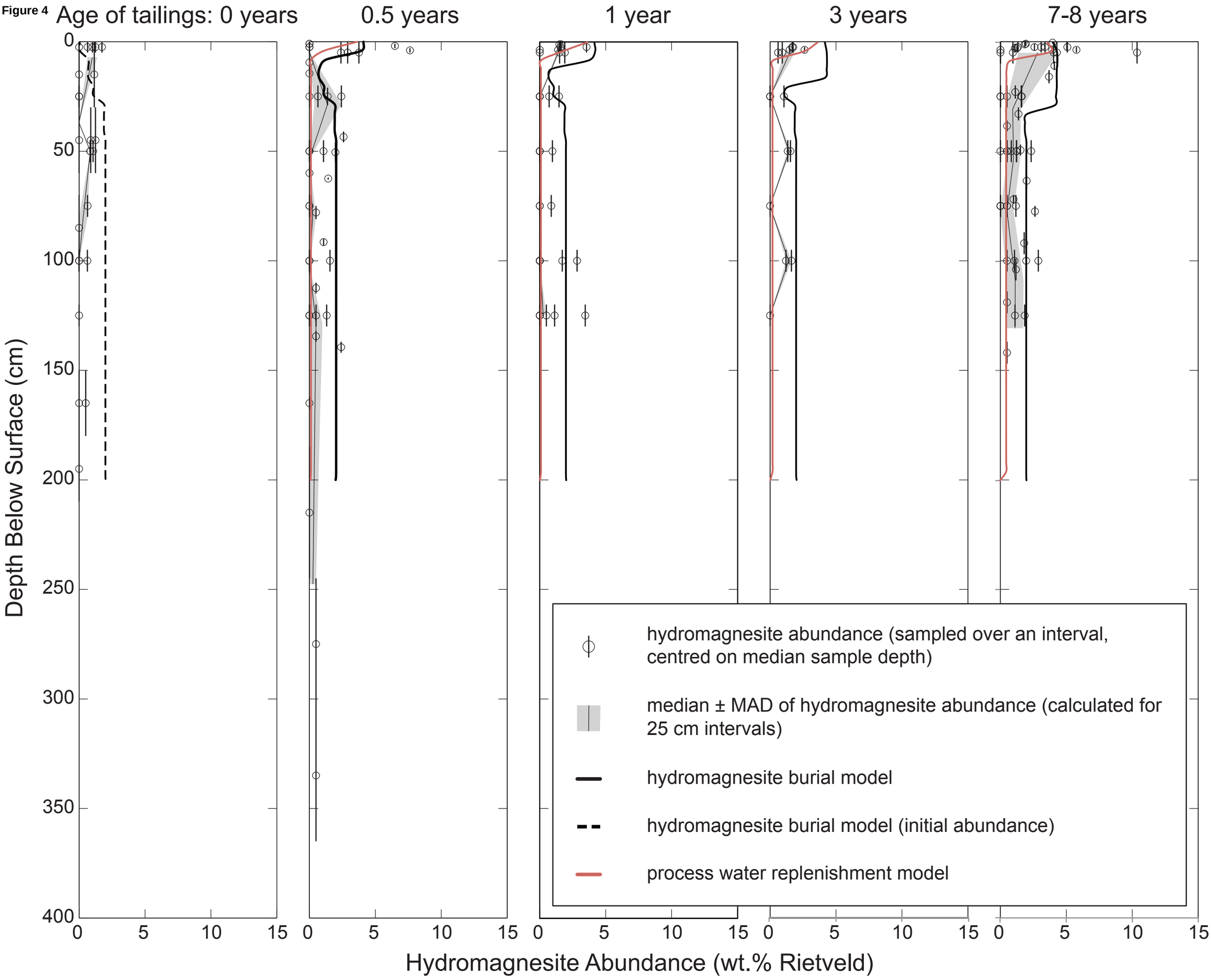
Age of tailings: 0 years
0.5 years
1 year
3 years
7-8 years
Depth Below Surface (cm)
0
50
100
150
200
250
300
350
400
0
5
10
15
Hydromagnesite Abundance (wt.% Rietveld)
hydromagnesite abundance (sampled over an interval, centred on median sample depth)
median ± MAD of hydromagnesite abundance (calculated for 25 cm intervals)
hydromagnesite burial model
hydromagnesite burial model (initial abundance)
process water replenishment model

Figure 5

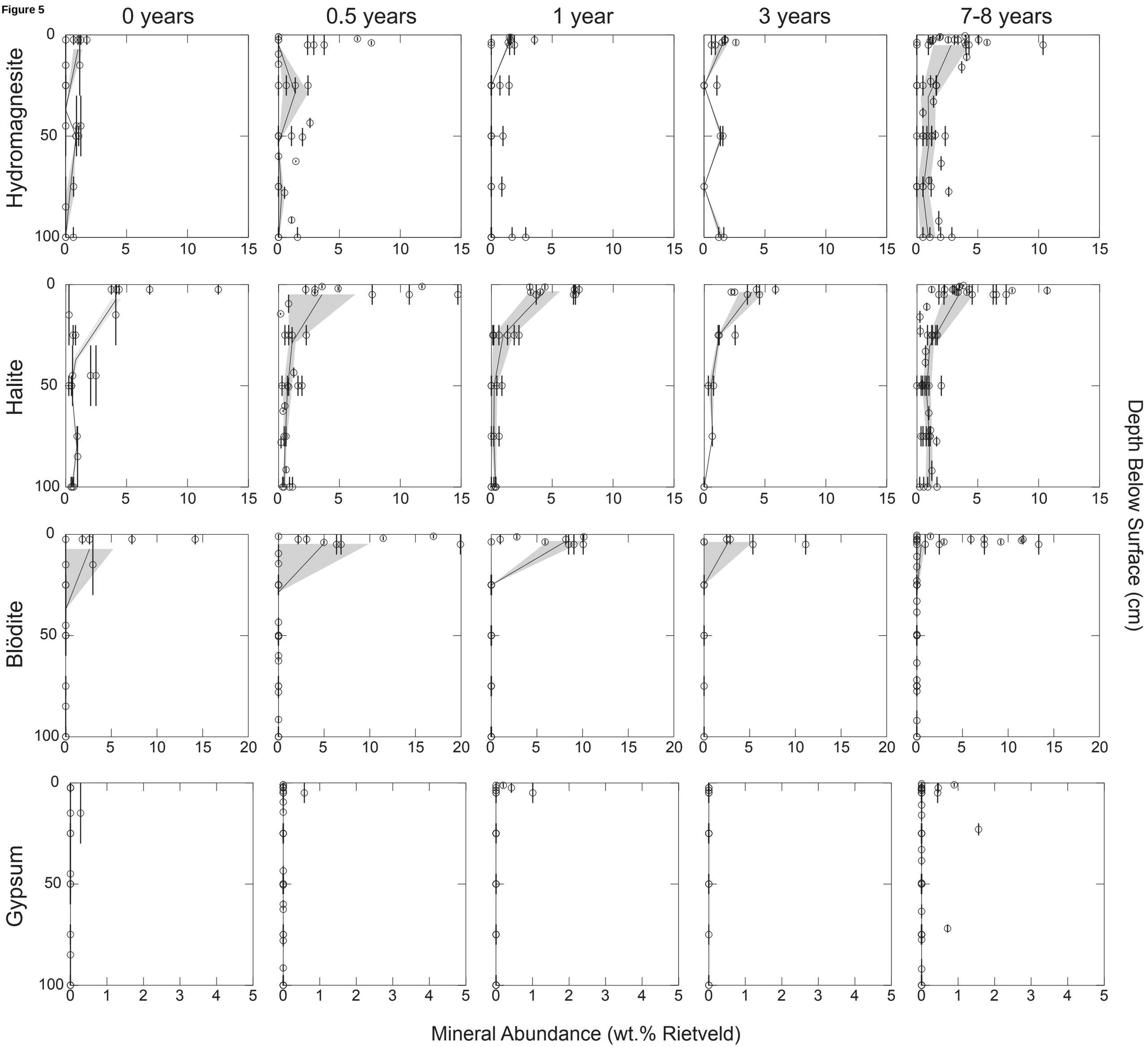
0 years
0.5 years
1 year
3 years
7-8 years
Hydromagnesite
Halite
Blödite
Gypsum
Depth Below Surface (cm)
Mineral Abundance (wt.% Rietveld)

Figure 6

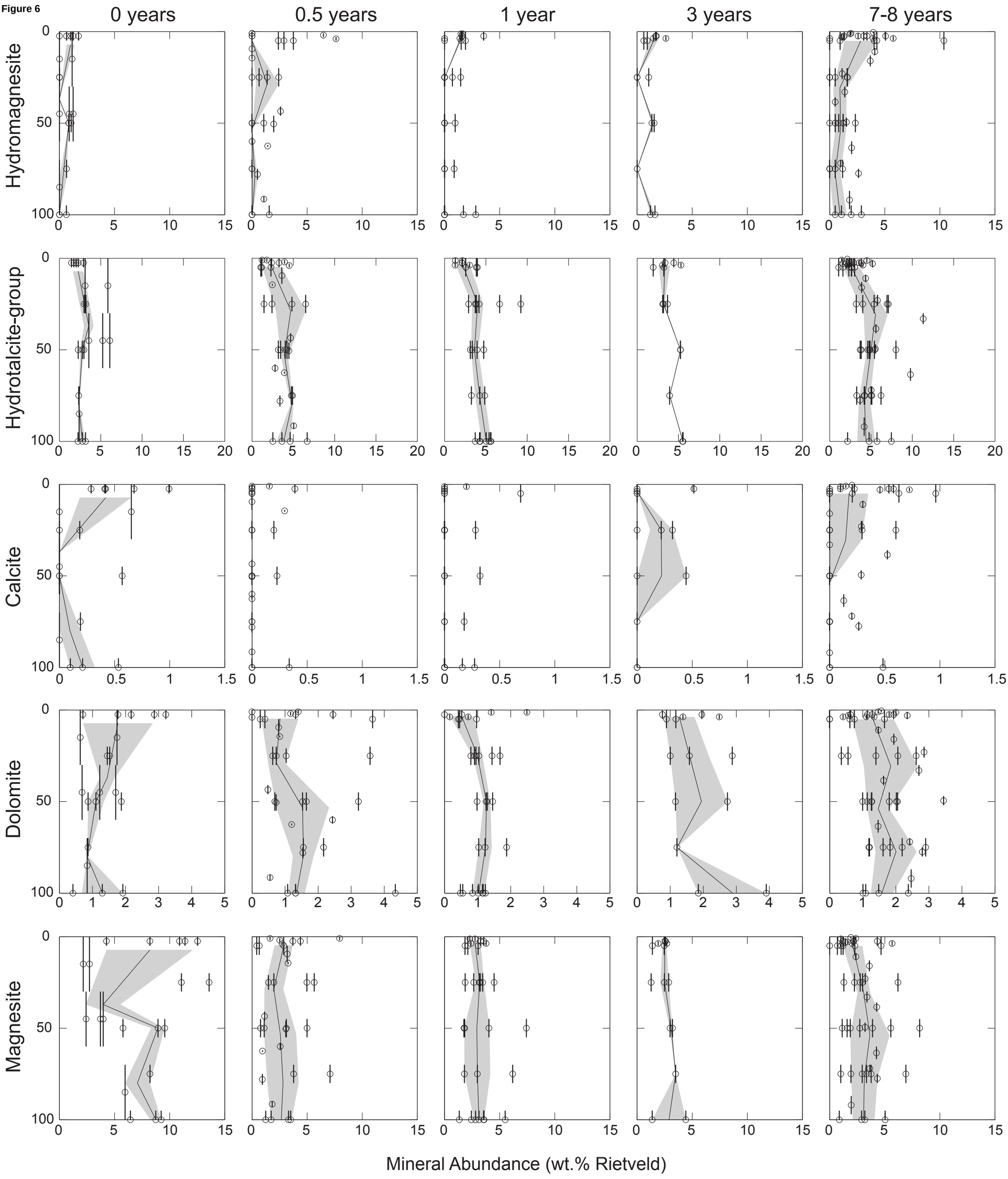
0 years
0.5 years
1 year
3 years
7-8 years
Hydromagnesite
Hydrotalcite-group
Calcite
Dolomite
Magnesite
Depth Below Surface (cm)
Mineral Abundance (wt.% Rietveld)

Figure 7

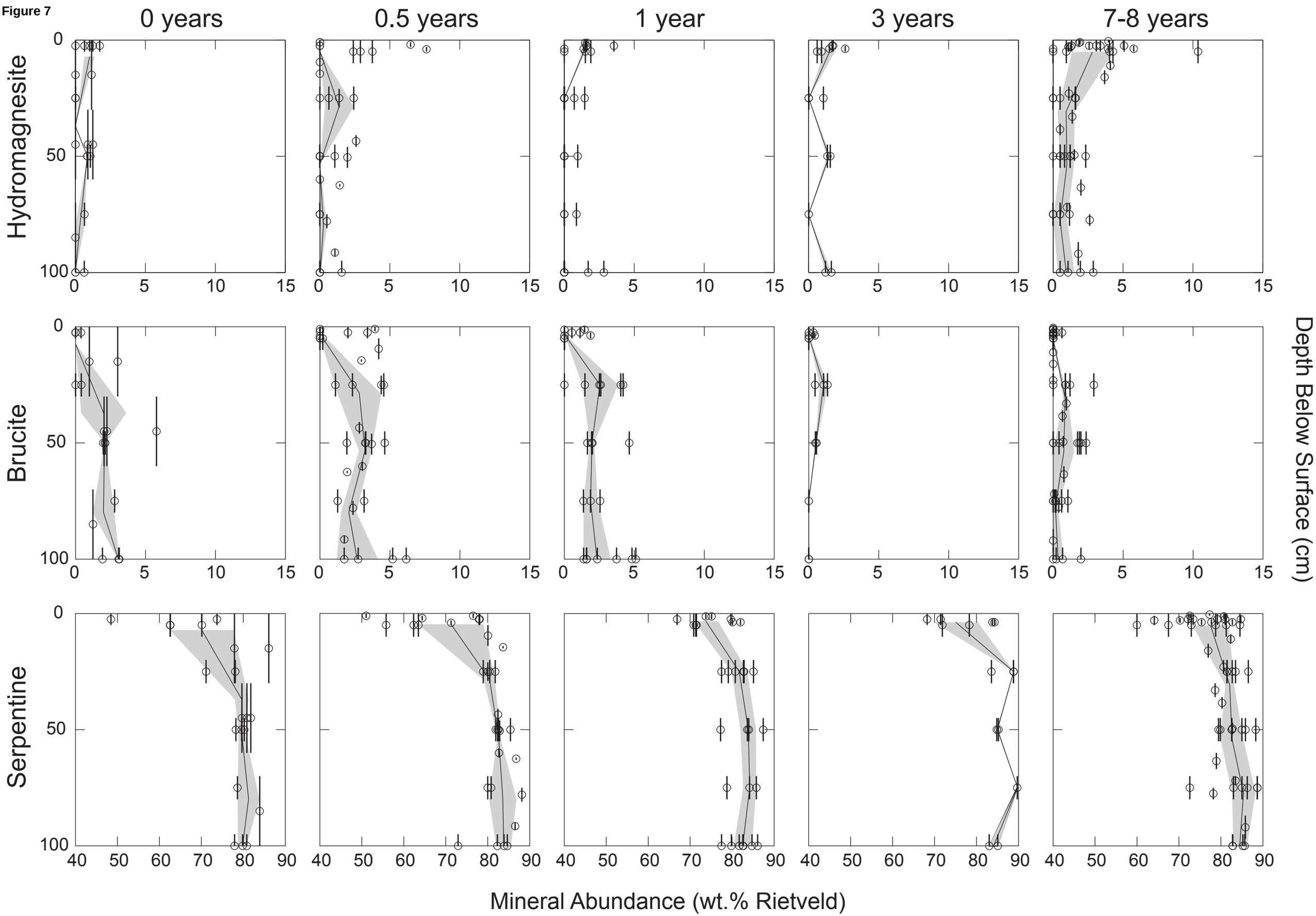
0 years
0.5 years
1 year
3 years
7-8 years
Hydromagnesite
Brucite
Serpentine
Depth Below Surface (cm)
Mineral Abundance (wt.% Rietveld)
0
50
100
0
5
10
15
40
50
60
70
80
90

Figure 8

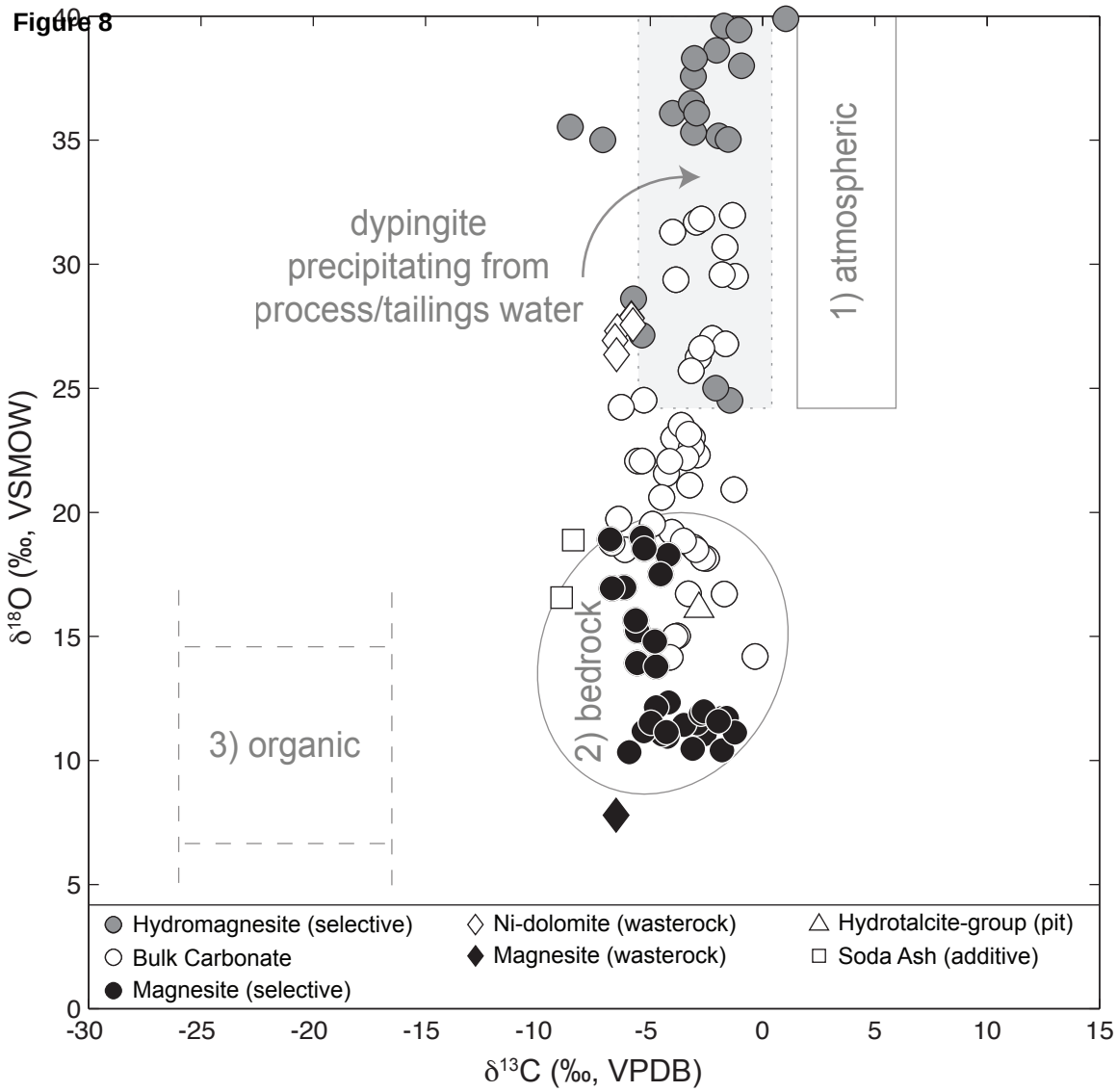
dypingite
precipitating from
process/tailings water
1) atmospheric
2) bedrock
3) organic
δ18O (‰, VSMOW)
δ13C (‰, VPDB)
40
35
30
25
20
15
10
5
0
-30
-25
-20
-15
-10
-5
0
5
10
15
Hydromagnesite (selective)
Bulk Carbonate
Magnesite (selective)
Ni-dolomite (wasterock)
Magnesite (wasterock)
Hydrotalcite-group (pit)
Soda Ash (additive)

Figure 9

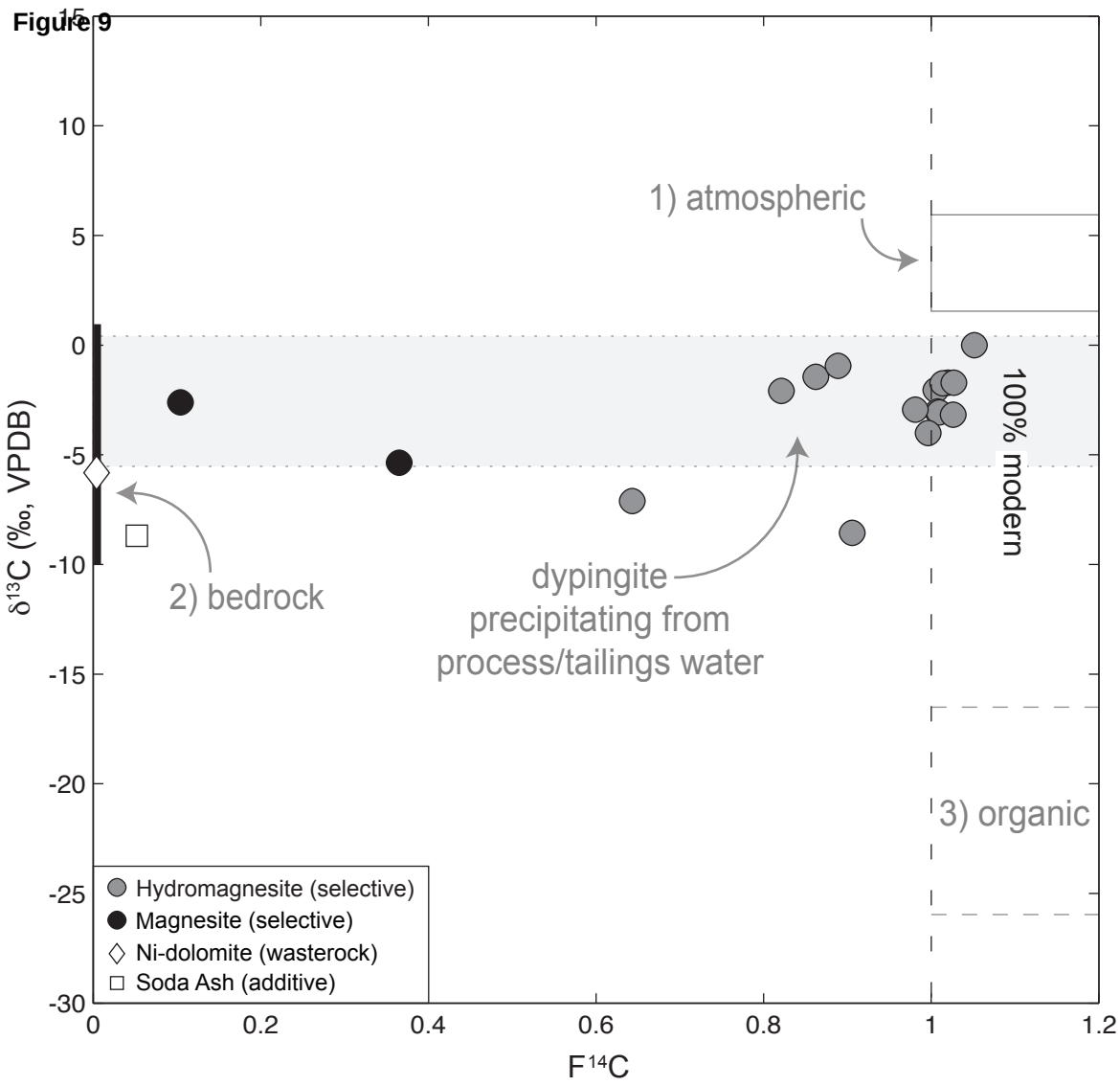
15
10
5
0
-5
-10
-15
-20
-25
-30
0
0.2
0.4
0.6
0.8
1
1.2
δ13C (‰, VPDB)
F14C
1) atmospheric
100% modern
2) bedrock
dypingite
precipitating from
process/tailings water
3) organic
Hydromagnesite (selective)
Magnesite (selective)
Ni-dolomite (wasterock)
Soda Ash (additive)

Figure 10

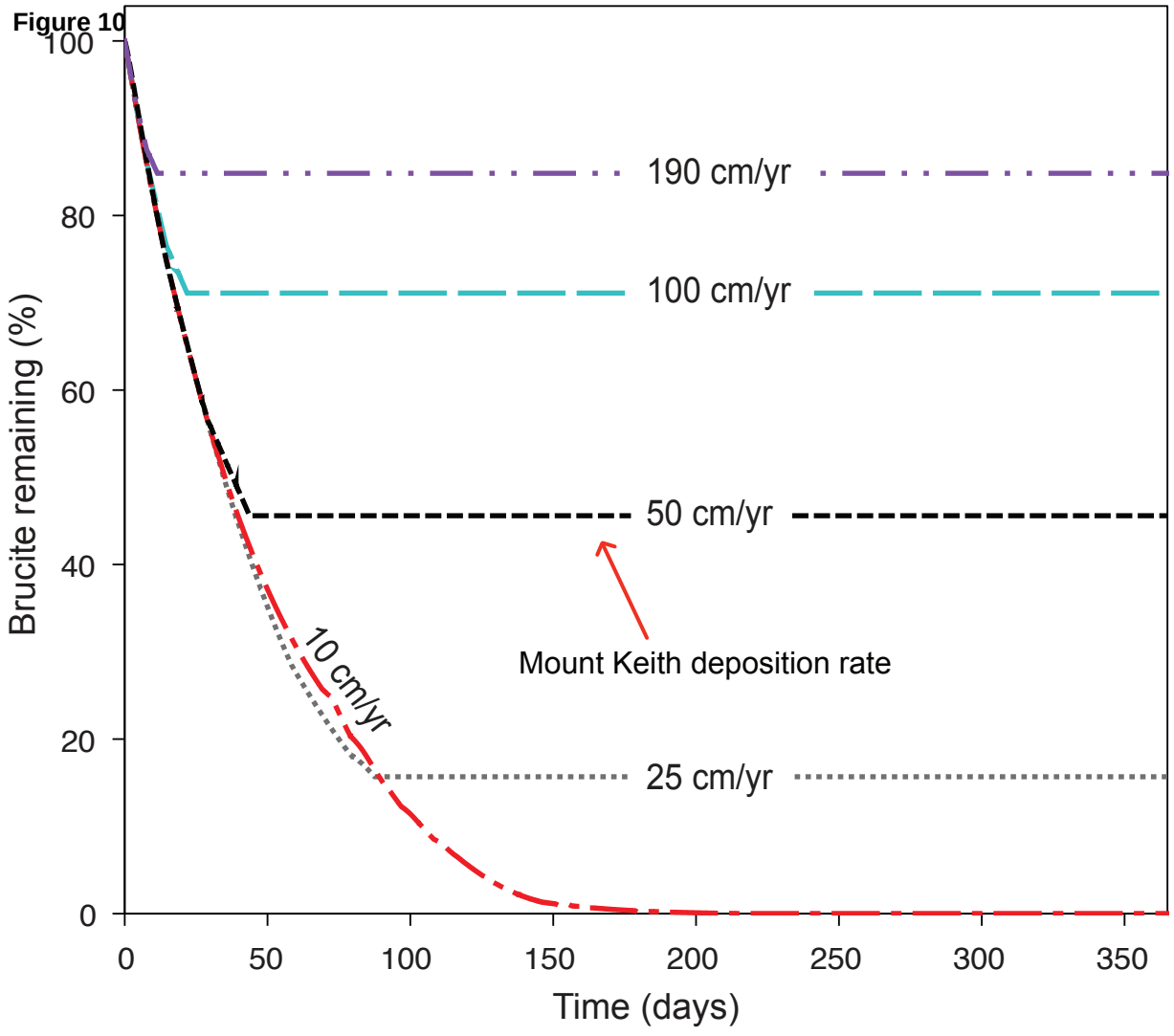
Brucite remaining (%)
100
80
60
40
20
0
0
50
100
150
200
250
300
350
Time (days)
190 cm/yr
100 cm/yr
50 cm/yr
Mount Keith deposition rate
10 cm/yr
25 cm/yr

Figure 11

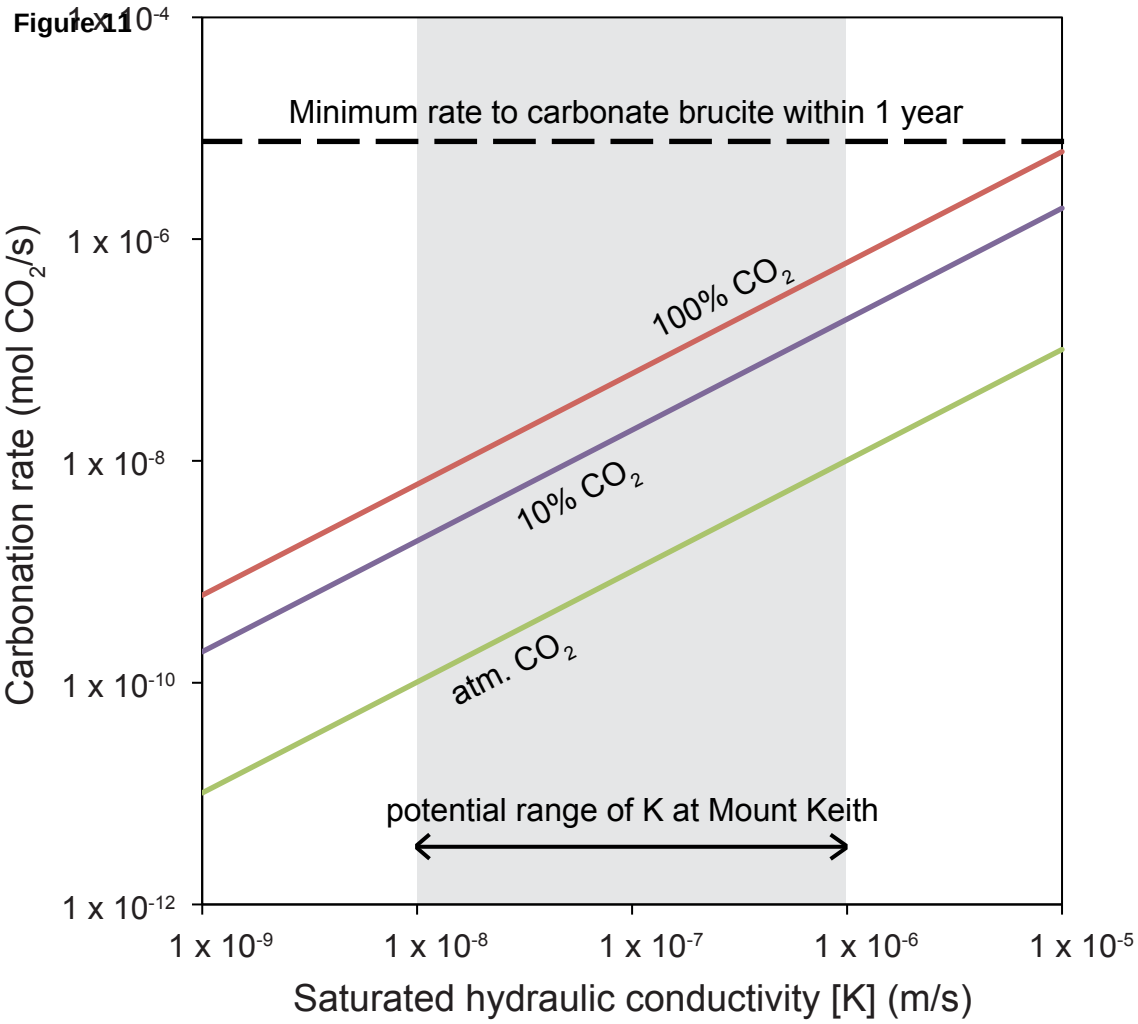
1 x 10-4
Minimum rate to carbonate brucite within 1 year
1 x 10-6
1 x 10-8
1 x 10-10
1 x 10-12
Carbonation rate (mol CO2/s)
100% CO2
10% CO2
atm. CO2
potential range of K at Mount Keith
1 x 10-9
1 x 10-8
1 x 10-7
1 x 10-6
1 x 10-5
Saturated hydraulic conductivity [K] (m/s)

Supplementary Material

Click here to download Supplementary Material: Mt Keith Supplemental V10.docx